CEEGS DELIVERABLE D3.1

CEEGS CYCLE, RELEVANT SYSTEM CHARACTERISATION

Summary:
This deliverable shows the main results of task 3.1 in the first 12 months of execution. It defines the main parameters and components integration within the base designs of the CEEGS project system. Two power scales, 5 MW and 100 MW, are considered for the analyses and designs. The deliverable defines the reference layouts and the main parameters of the cycle. The task 3.1 has evolved satisfactorily, and relevant results regarding the layouts' definitions and parameters have been obtained. They will allow advancing in the next steps within task 3.1 and the related tasks in WP3 and WP4. No delays or deviations are identified regarding the planned activities.

Authors:

Andres Carro, University of Seville
Ricardo Chacartegui, University of Seville

Funded by
the European Union

Title:	Deliverable 3.1 – CEEGS cycle, relevant system characterisation
Lead beneficiary:	USE
Other beneficiaries:	
Due date:	31/10/2023
Nature:	Public
Diffusion:	All partners
Status:	Working Document
DOI:	
License information:	
Recommended Citation:	A. Carro, R. Chacartegui, The Horizon Europe CEEGS project: Deliverable 3.1 – CEEGS cycle, relevant system characterisation, University of Seville
Related Data:	
ORCID:	
Document code:	CEEGS_D.3.1

Revision history	Author	Delivery date	Summary of changes and comments
Version 01	NN	26.10.2023	
Version 02	NN	27.10.2023	
Final version	NN	31.10.2023	

Approval status				
	Name	Function	Date	Signature
Deliverable responsible	Andres Carro			
WP leader	Ricardo Chacartegui			
Reviewer				
Reviewer				
Project Coordinator	Ricardo Chacartegui			

Funded by the European Union. Views and opinions expressed are, however, those of the author(s) only and do not necessarily reflect those of the European Union or CINEA. Neither the European Union nor the granting authority can be held responsible for them.

Table of contents

Figures

Tables

Executive summary

Deliverable D3.1 defines the main parameters and components integration within the base designs of the CEEGS project system. Two power scales, 5 MW and 100 MW, are considered for the analyses and designs to identify potential differences between applications, involved processes and components.
It presents the results of the first part of Task 3.1, executed in the first twelve months of the project. These results provide the framework for the specific design of components in Task 3.2, and they are used in subsequent tasks within WP3 and WP4. Processes and components are modelled and simulated using simulation software with characteristics providing analyses oriented to different applications/solutions within the project. Models for optimised parameters values, components integration and preliminary surface component-geological loop have been developed in Engineering Equation Solver (EES) and Python. These results provide the framework for the design of components and operation modes. They are based on well-established component models, including heat transfer, pressure losses, turbomachinery, and cycle thermodynamics. They have been used to evaluate the cycle and component performance in different charge and discharge scenarios from a preliminary definition of available components and integrations, advancing in the definition of the optimised operation and systems and processes integrations.

Key sections of the deliverable include:

- Section 3 defines the main characteristics and the principle of operation of the transcritical CO_2 cycles and the geological storage of the CEEGS system used in the rest of the tasks.
- Section 4 describes the models and the main assumptions considered for the numerical simulations presented in the next section.
- Section 5 analyses the characteristics of the transcritical CO_2 cycles, including thermal exchanges and the impact of CO_2 pressure values on the high side. The high values of round-trip efficiency correspond to higher CO_2 pressure values during both the charging and discharging phases, imposing the thermodynamic cycle's shape. This relationship remains consistent regardless of the plant's size. The high-efficiency cases, above 50%, include all combinations of pressure on the high-temperature side of the charging and discharging phase above 160 bar, and some combinations for even higher pressures, such as the case of 140 bar in discharging for 180-240 bar in the charging phase and the case of 120 bar in discharging for 220-240 bar in the charging phase. The preliminary integration of the surface system with the geological storage based on salt cavities and the impacts on the transcritical CO_2 cycles and cycle operation are assessed. They define the reference cases and the range of parameters for the following tasks within WP3 and WP4.
- Section 6 presents the first design of heat exchangers, analysing preliminary integration compatible with the defined design parameters set. They are designed for maximum shell and tube pressures, obtaining global transfer coefficients within 150-800 W/m^2K range. The results of the preliminary design of heat exchangers are satisfactory at the different power ratings, showing the feasibility of the defined integrations.

The first period of task 3.1 has evolved satisfactorily, and relevant results regarding the layouts' definitions and parameters have been obtained. They will allow advancing in the next steps within task 3.1 and the related tasks in WP3 and WP4. No delays or deviations are identified regarding the planned activities. The parameters and integrations defined have set the specifications for the definition of main components and subsystems (heat exchangers and turbomachinery, tanks, and others) to be performed in the second part of task 3.1. Their definition will interact with Task 3.2, cycle performance optimisation (charge/discharge cycle operation, circulating fluid volumes) and with Task 3.4, CO_2 plume formation. The values of parameters and the layouts will be updated within an iterative process that comprises these tasks, revising the optimised parameters and integrations as new results are obtained from the different parts that integrate the global concept.

Based on these specifications and analyses, the subsystems and components selected for integration in the different alternatives of the CEEGS cycle will be studied and optimized at the component level. The final results of the iterative process will be presented in the updated version of this deliverable, D3.5, in month 24.

1. Introduction

The deliverable D3.1 defines the layouts, components integration and main values of parameters within the base designs of the CEEGS project system. It establishes the reference integration at a process-flow level for two different system power scales, 5 MW and 100 MW, to evaluate differences in the applications, processes and predesigns linked to the energy storage size, especially at the component analysis.
It presents the results for the first part of the execution of task 3.1 in the first twelve months of the project.

2. Objectives and Scope

D3.1 aims to define the components, reference layouts, and integration designs of the CEEGS system. They will be used in subsequent analyses and integrations of WP3, WP4 and WP5 tasks. The values of parameters and the layouts will be updated within an iterative process within task 3.1 and interacting with other tasks of WP3 and WP4, revising the optimised parameters and integrations as new results are obtained from the different parts that integrate the global concept.

Processes and components are modelled and simulated using simulation software with characteristics that provide analyses oriented to different applications/solutions within the project. Models for optimised parameters, components integration and preliminary surface component-geological loop have been developed in EES and Python. These results provide the framework for the design of components and operation modes. The surface system and the geological loop, including preliminary performance maps, are integrated with Ebsilon software. Heat transfer integration and heat exchanger predesigns are evaluated with Aspen software. It is an integrated and iterative approach based on well-established component models that include heat transfer, pressure losses, turbomachinery, and cycle thermodynamics. This approach provides the capacity for evaluating different charge and discharge scenarios under a preliminary definition of available components and integrations.

The deliverable develops a detailed study of CO_2 transcritical cycles in the cyclic charge /discharge phases. An optimization of the heat exchange with high and low-temperature storage is performed. As a first approach, CO_2 geological storage is included in salt cavities. Preliminary sizing and design of heat exchangers are performed.

A detailed analysis of cycle optimization is performed, evaluating the most suitable high-temperature pressure range for round-trip efficiency, including studying thermodynamic properties using different databases (using EES and the CoolProp python library). At this stage, thermal energy storage is based on pressurized liquid water as high-temperature sensible heat storage and ice as low-temperature latent heat storage. The preliminary design of low-temperature latent heat exchangers (LT-hx) and high-temperature sensible heat exchangers (HT-hx) for a 5 and 100 MWe power plant, which can operate in both charging and discharging phases, is carried out. In the high-temperature exchanger, the sensible heat exchange of CO_2 under supercritical conditions and water is considered under the abovementioned conditions. In the case of the low-temperature exchanger, a first approximation is made, maintaining the conditions previously analysed of CO_2 phase change under subcritical conditions at a temperature close to 0 ºC.

These parameters and integrations set the operation conditions for the definition of main components and subsystems (heat exchangers and turbomachinery, tanks,…) required in Task 3.2, cycle performance optimisation (charge/discharge cycle operation, circulating fluid volumes) and in Task 3.4, CO_2 plume formation. Based on these results, subsystems and components are selected for integration in the alternative layouts of the CEEGS cycle will be studied and optimized at the component level. Different heat exchanger designs are evaluated for specific CEEGS conditions.

Likewise, the designs of the considered turbomachinery will be assessed, addressing relevant challenges for turbines and compressors. Parameter values and integrations will be updated within the iterative process involving these tasks, revising the optimised parameters and integrations as predesigns components are obtained. These models and results also provide the conditions and tools for the CEEGS plant digital twin with interconnected data and embedded operational documents. This preliminary analysis for component design is extended for process optimization in Task 4.1 Integrated CEEGS digital models and the following tasks within WP4.

In the second part of task 3.1, the subsystems and components selected for integration into the different CEEGS cycle alternatives will be studied and optimized at the component level (heat exchangers, turbomachinery, thermal storage tanks and others) for the specific conditions of CEEGS. Alternative layouts will be evaluated regarding integration, subsystems and components, heat recovery, integrated system flows, multi-stage compression, and incorporation of refrigeration cycles. The final results of the iterative process will be presented in the updated version of this deliverable, D3.5, in month 24.

3. Definition of the reference CEEGS cycle

This section defines the key elements of the CO_2 electrothermal and geological energy storage system used to define the reference cases, describing the operation principles and main assumptions.

3.1 Principle of operation

The storage and subsequent retrieval of electrical energy through the CO_2-based Electrothermal Energy and Geological Storage (CEEGS) system rely on a reversible heat pump. During the charging process, electrical energy is converted into stored thermal energy. Conversely, during the discharge process, the stored thermal energy is converted back into electricity, which can then be fed into the grid, Figure 1.

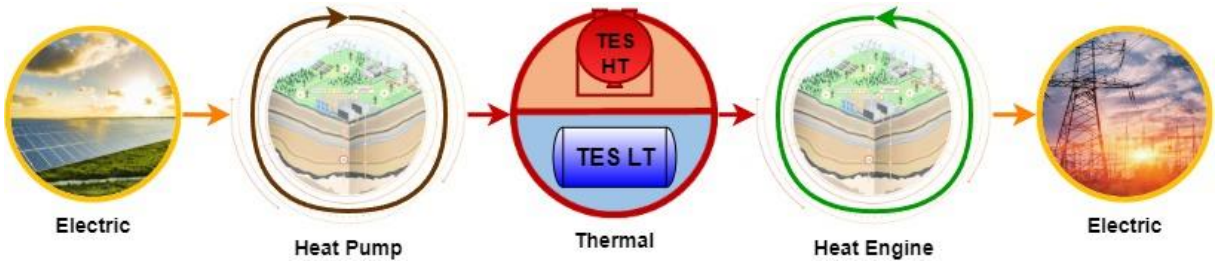

Figure 1. Schematic of electrical energy conversion using a CO_2 reversible heat pump and high and low-temperature thermal storage.

Carbon dioxide as the working fluid in a reversible heat pump of a Carnot battery has relevant advantages. Apart from its outstanding thermal and transport properties and wide availability, its integration potential with capture and storage plants adds significant value to the system. CO_2 transport and storage costs drop when CO_2 is in supercritical conditions [1,2].

Considering transcritical CO_2 cycles as the basis for the reversible heat pump, supercritical heating or cooling occurs on the high-pressure side, followed by a phase change on the low-pressure side. The high CO_2 pressures necessary for achieving the supercritical CO_2 state (above 70 bar) enable smooth integration with a CO_2 storage system in geological formations. These elevated CO_2 pressures in transcritical cycles are utilized in the injection/extraction processes into and from underground geological formations (Figure 2). CO_2 has adequate physical and chemical characteristics for its

geological integration, promoting synergetic integration between the Carnot battery and the geological plumes integration.

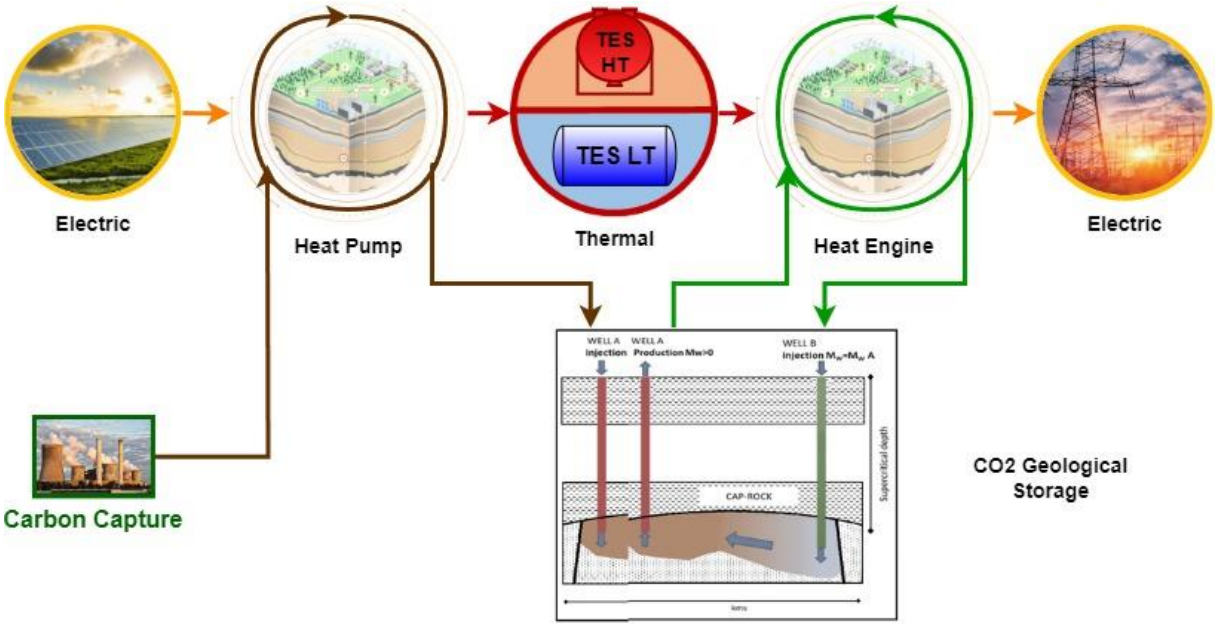

Figure 2. Schematic of including CO_2 geological storage in the electrothermal energy storage system [3,4]**.**

CEEGS system enables the storage of electricity from renewable sources while facilitating the long-term storage of CO_2 in underground formations. Moreover, the system could offer additional advantages, such as a partial geothermal gain and the permanent sequestration of a portion of CO_2 underground, as discussed in references [3,4].

3.2 Integration of transcritical cycles and thermal energy storage

3.2.1 Thermal energy storage system fluids

The selection of thermal storage fluids is determined by the specific features of CO_2 transcritical cycles, governing both the charging and discharging stages. Each stage comprises a high-pressure point, where supercritical heating/cooling occurs, and a low-pressure point that defines the phase change expansion line. The CEEGS concept requires high-temperature thermal storage within a temperature change of about 20-200 ºC and low-temperature thermal storage below 30 ºC, the critical temperature of CO_2. At this stage, focused on establishing the reference cases for defining the processes, components and operation, only water is considered for thermal storage because of its favourable characteristics (abundance, non-toxicity, cost, etc.). Other storage materials will be considered in the analyses of the second part of task 3.1.

Table 1. Fluids considered for thermal storage

High-temperature TES	Temperature Range [ºC]	Pressure[bar]
Water (liquid)	20-200	1-12
Low-temperature TES	**Temperature[ºC]**	**Pressure[bar]**
Ice	0	1

Liquid water for HT-TES.
Due to CO_2's critical temperature of approximately 31 °C, liquid water is firstly considered for high-temperature Thermal Energy Storage (HT-TES). Liquid water possesses a remarkably high heat capacity, resulting in a relatively high energy storage density both in terms of volume and mass. Moreover, water exhibits good heat transfer and heat transport characteristics [1,5]. It offers clear advantages concerning environmental availability, lack of toxicity, non-flammability, non-corrosiveness, and other chemical properties. However, its temperature range is relatively limited; it undergoes a phase change to solid at 0 °C and transitions to a gaseous state at around 100°C under atmospheric pressure.
Pressurized hot water TES broadens the temperature range for heat exchange operating with water in the liquid state. Increasing the pressure raises the boiling point significantly while the solidification point remains relatively stable, allowing for effective heat exchange into a broader temperature range.

Ice melting as LT-TES.
As the first case of study, ice (water slurries) is considered for Low-Temperature Thermal Energy Storage (LT-TES) due to CO_2's critical temperature and the need for a phase change in TES to achieve latent heat transfer effectively [3,6]. The phase change from water to ice occurs at 0 °C, aligning with the CO_2 phase change (CO_2 transitions at about 35 bar and 0 °C). Consequently, downstream pressures in the CO_2 system will be approximately around this value.
Ice slurries can be generated using various methods, such as evaporative technologies [1,7].

3.2.2 Integration of temperature profiles

The transcritical CO_2 cycle involves a phase change on the low-pressure side (evaporator or condenser). The implementation of thermal energy storage between the state change of each phase requires that the temperature of the low-temperature storage (LT-TES) must be between the two. Using low-temperature thermal storage based on latent heat through a phase change in the storage will result in more efficient integrations [3,6], Figure 3.

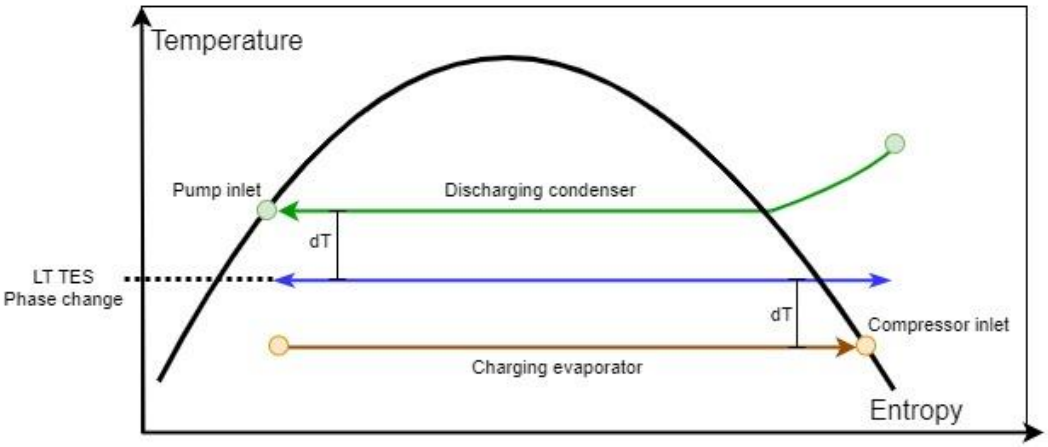

Figure 3. An example of an efficient latent heat transfer integration. Both temperature curves are parallel and close, reducing exergy losses.

In the high-pressure side heat exchanges, the characteristics of the supercritical state of CO_2 and the shape of the associated temperature profiles must be considered for adequate integration and higher efficiencies [1,3], Figure 4. The temperature variation of a liquid under subcritical conditions follows a linear progression. This aspect is crucial to consider when designing heat exchangers. The placement

of the pinch point should align with the tangent line on the curves and run parallel to the HT-TES evolution line.

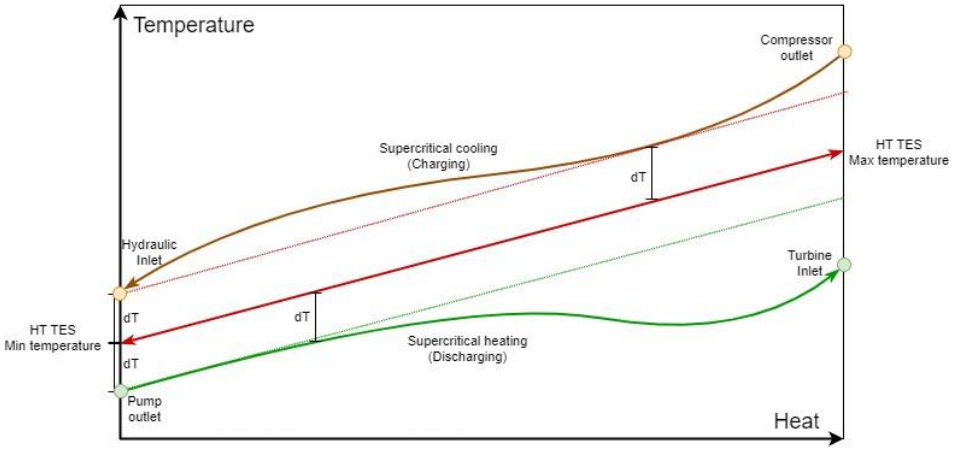

Figure 4. An example of an adequate integration of temperature-heat transferred on the high-temperature side. Both temperature curves are very close, reducing exergy losses.

3.3 Integration of the geological storage of CO_2

Geological CO_2 storage is crucial for deploying carbon capture and storage (CCS) technology. CCS involves capturing CO_2 emissions from industries and combustion processes, transporting the captured CO_2, and injecting it into deep and stable geological formations, where it is permanently stored.

As of 2022, there are 30 operational CCS facilities worldwide, with a capacity for injecting 42.5 million metric tons per annum (Mtpa) of CO_2. Additionally, 11 facilities are under construction, and over 150 are in various stages of development, potentially adding up to a total capacity of about 240 Mtpa of CO_2 [8]. However, to meet climate targets, the current rate of CO_2 storage, which stands at approximately 40 Mtpa, must increase significantly to reach capacities in the thousands of Mtpa [8].

According to d2.1, the CO_2 injection process is a matured technology that has been employed by the oil industry since 1972. Currently, and worldwide, the mass of annually injected CO_2 is above 40 Mt of CO_2 for enhanced hydrocarbon recovery (EOR) purposes primarily, or CO_2 capture and storage (CCS) as a climate mitigation technology secondarily. The selection of geological reservoirs for CCS purposes is well-established and documented. It applies to CEEGS, ensuring suitable porous and permeable reservoirs and very low permeability cap-rocks preventing CO_2 from ascending to the surface by buoyancy. However, CCS requires highly stable geological formations with outstanding characteristics for permanent sequestration. Different conditions are expected for the CEEGS technology, where only partial permanent sequestration is aimed, and the conditions of the reservoirs for closing the energy storage loop can be different.

The efficiency of the CEEGS with CO_2 underground injection and back-production depends mainly on pressure (P) and temperature (T) conditions at the reservoir and P-T variation between wellheads and bottomholes. They count on the allowable maximum and allowable pressure oscillations in the plumes/reservoirs and the charge-discharge strategies. Within these limits, from the energy storage point of view, the pressures are a function of the flow rates and well diameters but also of the length of the wells, i.e. of reservoir depths. The P-T changes within the well are particularly relevant for the back-production of CO_2 from the reservoir to ensure that the CO_2 saturation line is not reached and

two-phase flow does not occur in the producing well. This approach has been applied in D2.1 to porous media, either deep saline aquifers or depleted hydrocarbon fields and salt cavities.

4. CEEGS system modelling

4.1 Description and preliminary assumptions

Table 2 summarises the main assumptions used for the modelling and definition of the reference cases. Temperature lines on the CO_2 low-pressure side are determined by the LT-TES conditions, which set the pressures. The compression/expansion lines are established based on the equipment's isentropic performance [1,6], thereby defining the inlet conditions for the high exchanges.

At the high-temperature thermal exchange, the thermal storage system (HT-TES), a water-pressurised system, is considered to prevent phase change, ensuring the water liquid state is maintained to provide high energy storage density. In the design reference cases, this pressure corresponds to a temperature 10 °C above the compressor outlet temperature and aligns with the maximum CO_2 pressure considered in the analysis (240 bar). The CO_2 pressure range on the high-temperature side varies from 80 bar (slightly above the critical pressure to maintain the characteristics of the transcritical cycles) to 240 bar.

Table 2: Assumptions in the modelling of transcritical CO_2 cycles

		Units	Charging	Discharging
Minimum temperature difference (dT)	HT side	ºC	4	4
in heat exchangers for design	LT side	ºC	4	4
Isentropic performance of equipment	Compression	%	89-85	86-80
	Expansion	%	88	91-90
LT TES – **Ice** conditions	Pressure	Bar	1	1
	Temperature	ºC	0	0
HT TES – **Water** conditions	Pressure	Bar	1-12	1-12
	Temperature	ºC	10-180	10-180
Transcritical CO_2 cycles	Low pressure	Bar	31.3	38.7
	High pressure	Bar	80-240	80-240
Operating conditions	Operating time	Hours	10	0-10
	Electrical power	MW	5-100	5-100

For the detailed analysis of the CEEGS system cycles in its different operating modes, models have been developed in different numerical simulation software to take advantage of their capacities regarding the type of analysis, potential integrations with other tools and the use of different databases to compare and validate the results.

Table 3. Software and data bases in numerical modelling

Software	Software ref	-	Data Base Ref
Engineering Equation Solver (EES)	[9]	Properties CO_2	[10–12]
		Properties Ice	[13,14]
		Properties Water	[13,15]
Python		CO_2 and Water properties	CoolProp library [16]
Ebsilon Professional	[17]	Water properties	IAPWS-IF97 [18]

		CO_2 and R-22 properties	REFPROP (NIST) [19]
Aspen Plus & Aspen HYSYS	[20,21]	Substance properties Heat exchanger design	Aspen properties [22] Aspen Exchanger Design & Rating (EDR) [23]

4.2 Analysis of CO_2 transcritical cycles. Definition of the reference cases.

For the definition of the reference cases, a mathematical model has been developed in the commercial software EES [9] to solve mass and energy balances and adjust the temperature-heat exchange profiles. Thermodynamic properties are calculated from different databases for CO_2 [10–12], ice [13,14] and water [13,15].

4.2.1 Reversible heat pump of CO_2: closed cycle operation

This model comprises a heat pump for the charging phase (HP-Charging) and a thermal engine for the discharging phase (HE-Discharging). During the charging stage (1-2-3-4), electrical energy generated from renewable sources is converted into thermal energy. This thermal energy is stored as sensible heat on the high-temperature side (HT-TES) and latent heat on the low-temperature side (LT-TES). In the discharge phase (5-6-7-8), the thermal energy previously stored is utilized to generate electricity, Figure 5.

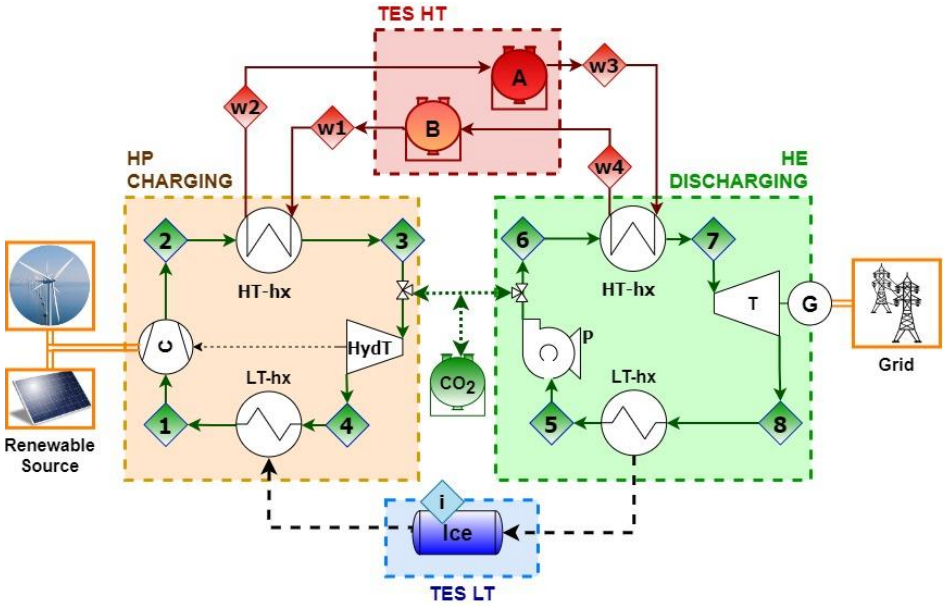

Figure 5: Conceptual scheme of the basic configuration of the thermoelectric energy storage system using transcritical CO_2 cycles (TEES- CO_2) and storage in ice and hot water.

The power elements are modelled according to the isentropic performance set in the assumptions. At the same time, the heat exchanges have been optimized to establish the minimum temperature difference from the same table. The size of the equipment depends on the electrical power of the charging and discharging phases and the number of hours considered for the operation of the system.

4.2.2 Integration of geological storage

Geological storage is integrated into the system while preserving the distinct nature of the two stages:

- The charging stage, where renewable electrical energy from sources like wind power plants or photovoltaic fields is converted into thermal energy via a heat pump.

- The discharging stage where the stored thermal energy is utilized in a heat engine to generate electricity.

Each stage operates using a separate CO_2 transcritical cycle, and thermal energy is stored as sensible heat in pressurized water and as latent heat through the phase change of ice.

The system operates in an open cycle, incorporating energy storage and the geological storage of captured CO_2. This integration leverages the favourable conditions of transcritical CO_2 cycles for efficient geological storage (Figure 6).

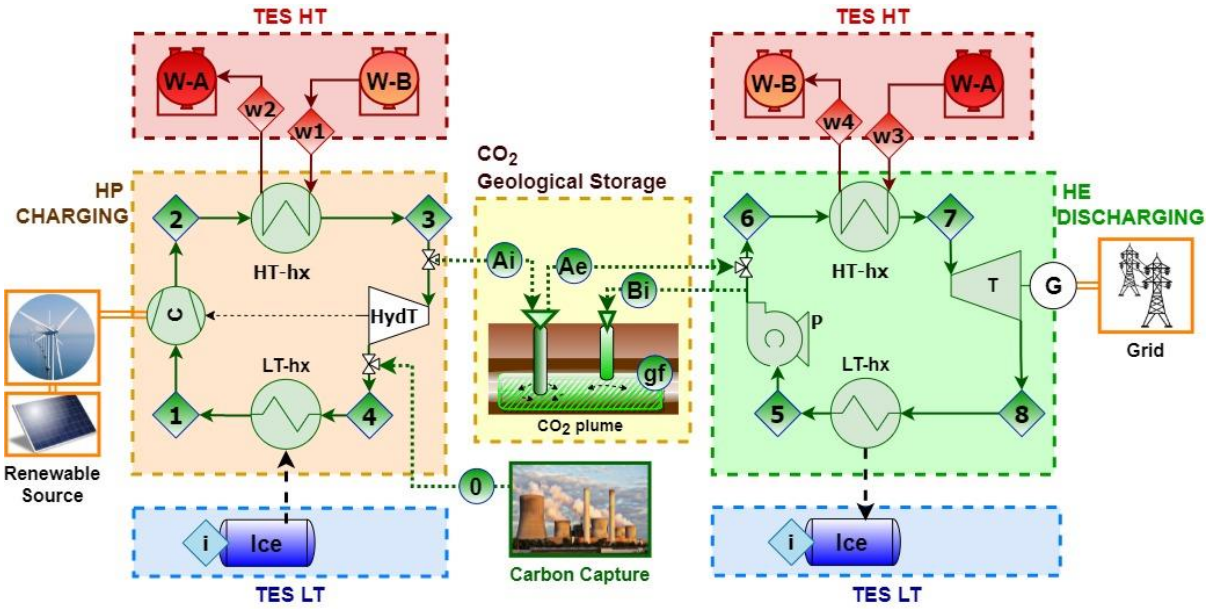

Figure 6. CEEGS reference case. Conceptual scheme of the CEEGS system incorporating electrothermal energy storage and CO_2 geological storage.

The processes involving supercritical CO_2 cooling (2-3) during the charging phase and supercritical CO_2 heating (6-7) during the discharging phase, occurring on the high-temperature side, define the parameters for CO_2 injection and extraction into geological formations, respectively. The CO_2 injection/extraction conditions in geological formations impact the configuration of the transcritical cycles of the reversible heat pump (indicated as 3* and 6* in Figure 7). These conditions influence the thermal energy stored or extracted from ice reservoirs and hot water (w1* and w4* in Figure 7).

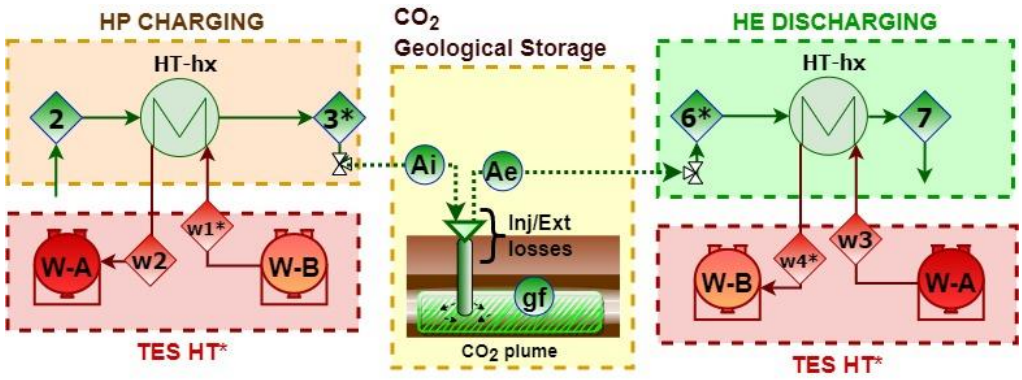

Figure 7. Conceptual scheme of the geological storage integration in the high-temperature side of transcritical cycles – EES model.

As constraints on CO_2 pressure within underground geological formations (CO_2 plume), a pressure range of 80-200 bar is considered. This range is set below the CO_2 pressure during the supercritical cooling phase of the charging process (210 bar), ensuring a consistently supercritical state.

In terms of temperature, the range is determined by the boundaries of the pressure range and the CO_2 entropy limits within the described transcritical cycles. The upper limit corresponds to the turbine inlet conditions during the discharging phase (7). The lower limit aligns with the inlet conditions during the expansion phase of the charging process (3), **Figure 8**.

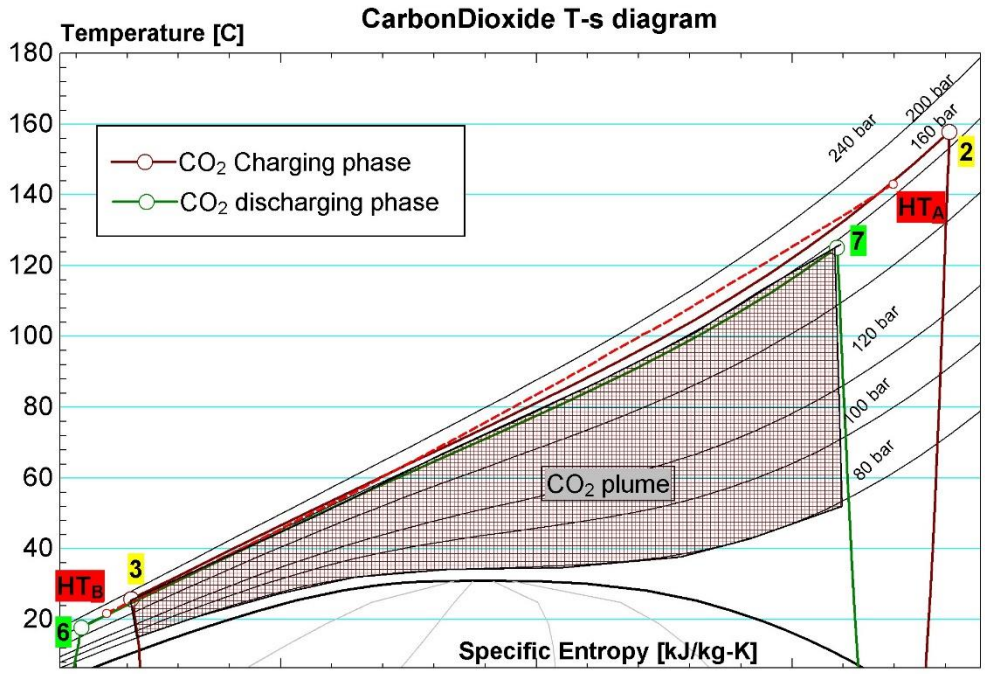

Figure 8. CO_2 geological storage plume conditions – EES model.

The conditions at the compressor outlet during charging (2) and the turbine inlet during discharging (2) are assumed to be constant. However, the conditions of the CO_2 plume are allowed to vary, spanning the entire area depicted in the Figure. These variations influence the CO_2 inlet conditions during the expansion phase of the charging process (from 3 to 3*) and the compressor outlet conditions during the discharging phase (from 6 to 6*).

For establishing injection/extraction conditions at the surface, a pressure loss of 20% is factored in both during CO_2 injection into the geological formation and during the extraction of stored CO_2. It is assumed that the conditions of the CO_2 plume stored within the underground geological formation remain stationary.

Table 4. Main assumptions for the analysis of injection/extraction conditions.

Reference		Units	Value
CO_2 plume	Pressure	bar	80-200
	Temperature	ºC	15-125
Pressure losses	Injection	%	20
	Extraction	%	20

4.2.3 Indicators

To quantify the efficiency of the charging (η_{HP}) and discharging (η_{HE}) phases separately, and the roundtrip efficiency (η_{TEES}), the efficiency indicators of equations 1-3 are defined.

$$(1)\ \eta_{HP} = \frac{\dot{Q}_{HT-hx,charging} + \dot{Q}_{LT-hx,charging}}{\dot{W}_C - \dot{W}_{HydT}}$$

$$(2)\ \eta_{HE} = \frac{\dot{W}_T - \dot{W}_P}{\dot{Q}_{HT-hx,discharging} + \dot{Q}_{LT-hx,discharging}}$$

$$(3)\ \eta_{TEES} = \frac{\dot{W}_T - \dot{W}_P}{\dot{W}_C - \dot{W}_{HydT}} \cdot \frac{t_{discharging}}{t_{charging}}$$

Where $\dot{Q}_{HT-hx}$ and $\dot{Q}_{LT-hx}$ refer to the thermal power in the high and low-temperature exchanges for each phase, charging and discharging. $\dot{W}$ is the power developed by the compression and expansion equipment, compressor (C), pump (P), expansion in charging (HydT) and gas turbine in discharging (T). The variable " t " refers to the operation time in each phase.

Efficiency indicators (Eqs. 4-6) are defined to quantify the impact of using the open-cycle mode of operation, both for the charging ($\eta_{HP}{}^{*}$) and discharging ($\eta_{HE}{}^{*}$) phases and the overall roundtrip efficiency ($\eta_{ETES}{}^{*}$), and to compare with the efficiency of the closed-cycle mode of operation (Eqs. 1-3).

$$(4)\ \eta_{HP}{}^{*} = \eta_{HP} \cdot \frac{h_{char}}{h_{char,tot}} + \frac{\dot{Q}_{HT-hx,charging}{}^{*} + \dot{Q}_{LT-hx,charging}{}^{*}}{\dot{W}_C{}^{*} - \dot{W}_{Exp}{}^{*}} \cdot \frac{h_{char}{}^{*}}{h_{char,tot}}$$

$$(5)\ \eta_{HE}{}^{*} = \eta_{HE} \cdot \frac{h_{dis}}{h_{dis,tot}} + \frac{\dot{W}_T{}^{*} - \dot{W}_{Comp}{}^{*}}{\dot{Q}_{HT-hx,discharging}{}^{*} + \dot{Q}_{LT-hx,discharging}{}^{*}} \cdot \frac{h_{dis}{}^{*}}{h_{dis,tot}}$$

$$(6)\ \eta_{ETES}{}^{*} = \frac{(\dot{W}_T - \dot{W}_P)\cdot h_{dis} + (\dot{W}_T{}^{*} - \dot{W}_{Comp}{}^{*})\cdot h_{dis}{}^{*}}{(\dot{W}_C - \dot{W}_{HydT})\cdot h_{char} + (\dot{W}_C{}^{*} - \dot{W}_{Exp}{}^{*})\cdot h_{char}{}^{*}}$$

The indicators depend on the number of hours in which the system operates in a closed or open cycle; h_{tot} is the total hours of charging (char) and discharging (dis), adding those that the system operates in each mode, the superscript "*" refers to the use of the open cycle operation mode, and $\dot{W}_{Exp}{}^{*}$, $\dot{W}_{Comp}{}^{*}$ is the expansion power in charging and compression power in discharging, respectively.

4.3 Integration of transcritical cycles and injection in salt cavities

A numerical model has been developed in Python. It adds to the previously described models the advantage of including specific models for the wells. It is designed for further integration with the tools to be developed in the next tasks of WP3 and WP4. This model uses the CoolProp library [16] to calculate substance properties. It is based on modelling a reversible heat pump, charging phase (HP-Charging; 1-2-3-4) and discharging phase (HE-Discharging; 5-6-7-8) by transcritical CO_2 cycles. The power equipment is defined by isentropic efficiency, and a minimum temperature difference optimizes the heat exchanges. This optimal temperature difference constraint considers the supercriticality of CO_2 on the high-temperature side, adjusting the hot water temperature – heat exchange profile between the CO_2 evolution lines.

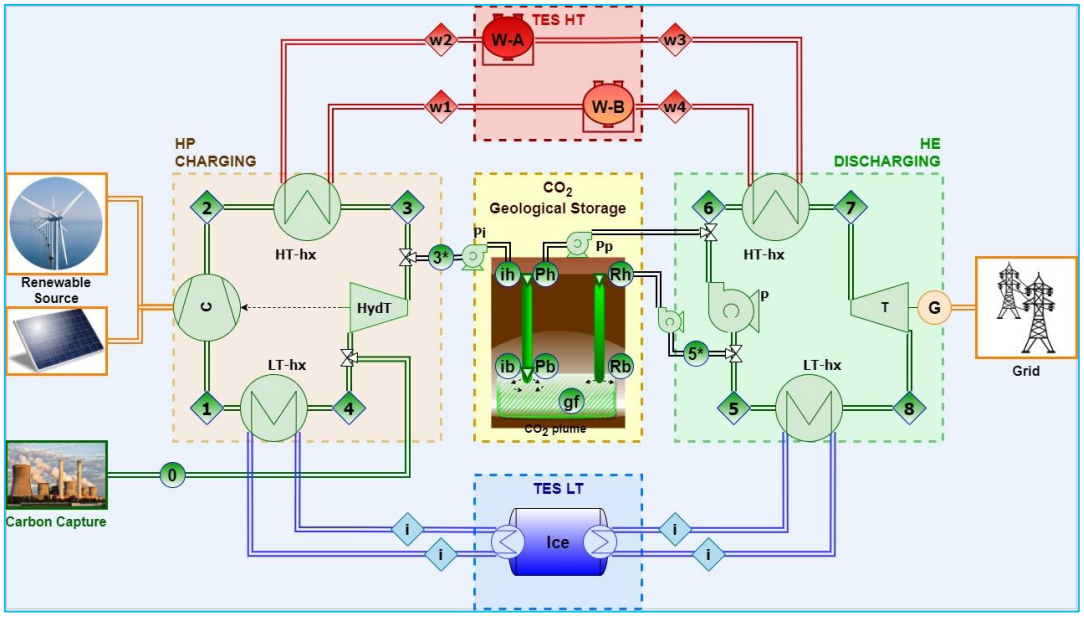

Figure 9. Python model. Conceptual scheme of the CEEGS system incorporating electrothermal energy storage and CO_2 geological storage into salt cavities.

The incorporation of geological storage is realized under the assumptions and considerations for salt cavities in deliverable d2.1. According to d2.1, experimental investigations on rock salt cores subjected to supercritical CO_2 pressurization showed that a pressure-driven opening of grain boundaries occurs in polycrystalline rock salt. Thus, a loss of tightness only occurs when the CO_2 pressure significantly exceeds the minimum principal stress (Minkley et al., 2022). The maximum storage pressure is limited by the minimum principal stress in the salt rock acting on the cavern roof, i.e. by the lithostatic pressure (Soubeyran et al., 2019). Therefore, the allowable pressures in salt caverns are considerably higher than those allowable in porous media, which are a function of hydrostatic pressure and are usually limited to 20 % of the cumulative pressure. The lithostatic pressure (MPa) is calculated as a function of the depth (m) of the top of the saline capacity, according to Eq 7:

$$(7)\ P_{lith}{}^{\text{salt,cavs}} = 0.022 * \text{Depth}^{salt,cavs}$$

Following the maximum and minimum pressure values used as pressure limits in the CAES industry and defined by Allen et al. (1982) (and also followed by Soubeyran et al. (2019)) as:

$$(8)\ P_{min}{}^{\text{salt,cavs}} = \max\left(0.3 * P_{lith}{}^{\text{salt,cavs}}; \text{P}_{CO2}^{Crit}\right)$$

$$(9)\ P_{max}{}^{\text{salt,cavs}} = 0.8 * P_{lith}{}^{\text{salt,cavs}}$$

This minimum pressure is necessary to avoid cavity closure. It is maintained by the cushion gas and is kept above the critical pressure to ensure the supercritical conditions of the CO_2 in the plume. To ensure supercritical CO_2 behaviour, considering different pressure and temperature gradients and operating the cavity close to the minimum pressure imposed by the cushion gas, the minimum salt cavity depth required would be 1200 m, while the maximum salt cavity depth would be the same as usually recommended for CAES or natural gas storage, 2500 m to avoid salt plasticity at high temperatures (Allen and Doherty, 1982).

For both porous media and salt cavity scenarios, the most relevant parameters related to the subsurface component are the pressure and temperature conditions in the charging phase (well

operating in injection mode) and the discharge phase (well back-producing CO_2). Using the salt cavity model (Eq. 10),

$$(10)\ \rho_a(C_a - R)\dot{T}_a + \frac{\dot{m_{in}}c_a}{V}(T_a - T_{in}) + \frac{RT_a}{V}(\dot{m_{out}} - \dot{m_{in}}) + \frac{h_c A_c}{V}(T_a - T_s) = 0$$

and the well flow model (equations 11-14), the average values in the salt cavity and the pressure loss in the back-producing well are obtained :

$$(11)\ h_i + \frac{v_i^2}{2} + gz_i = h_{i+1} + \frac{v_{i+1}^2}{2} + gz_i$$

$$(12)\ P_i + \frac{\rho_i v_i^2}{2} + \rho_i g z_i = P_{i+1} + \frac{\rho_{i+1} v_{i+1}^2}{2} + g z_{i+1}$$

$$(13)\ \dot{m} = \rho_i A v_i = \rho_{i+1} A v_{i+1}$$

$$(14)\ \Delta P = f\frac{L_{pipe}}{D}\frac{\rho v^2}{2} = f\frac{L_{pipe}}{D^5}\frac{8\dot{m}}{\rho\pi^2}$$

Table 5 summarizes the assumptions that have been taken into account in the salt cavity injection calculations

Table 5: Assumptions in single salt cavity injection

Depth (m)	500	1000	1250	1500	1750	2000	2250	2500
Lithostatic pressure (bar)	110	220	275	330	385	440	495	550
Maximum Pressure (bar)	88	176	220	264	308	352	396	440
Minimum Pressure (bar)	33	66	82.5	99	115.5	132	148.5	165
Supercritical state	No	No	Yes	Yes	Yes	Yes	Yes	Yes
Cavity temperature (ºC)	30	45	51	60	69	75	81	90

4.4 Injection with pressure controls

An additional mathematical model has been developed in the commercial software Ebsilon Professional [17]. It provides additional value regarding the integration of equipment's performance maps and equipment analyses, required in the second stage of task 3.1, with the main results to be delivered in d 3.5. At this stage, it allowed the studies of the integrated performance of surface/underground systems and the pre-design of operation for adequate pressure profiles evolution and control in the wells. For the calculation of the thermodynamic properties of the fluids, the databases IAPWS-IF97 [18] for water and REFPROP (NIST) [19] for CO_2 and R-22 have been used.

The model analyses the two operation modes: closed cycle and open cycle. Figure 10 shows the arrangement of the charging and discharging phases operating in a closed cycle, as a reversible heat pump, storing electrical energy in the form of thermal energy and generating electricity from the previously thermal energy stored. R-22 has been used as a substitute for ice in the modelling to ensure a phase change around 0 ºC, due to restrictions in the simulation software on the use of ice slurries as a heat exchange stream.

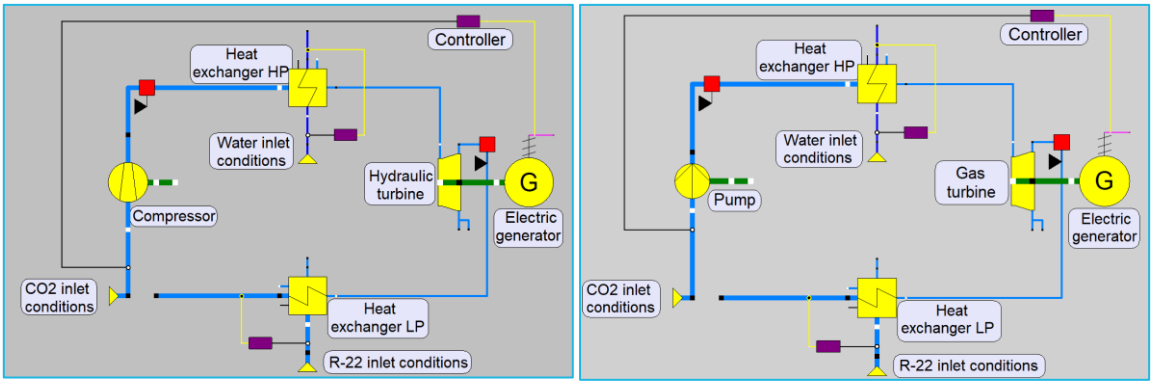

Figure 10. Ebsilon model. Conceptual scheme of the CEEGS system incorporating electrothermal energy storage

In the modelling of the open cycle, the same conditions have been imposed as in the closed case, and the values of the mass flow rates obtained as a result of the simulation of the closed-charging cycle have been fixed. In addition, the following assumptions regarding the injection well have been taken into account:

- Phase changes control within the well to avoid well damages
- Surface injection pressure of 90 bar.

Different cases are considered in the injection analysis, assuming a net electrical input power of 1, 5 and 100 MWe, and four injection cases for controlling the pressure profiles in the well: no restriction, one, two and three intermediate pressure reductions/dampers.

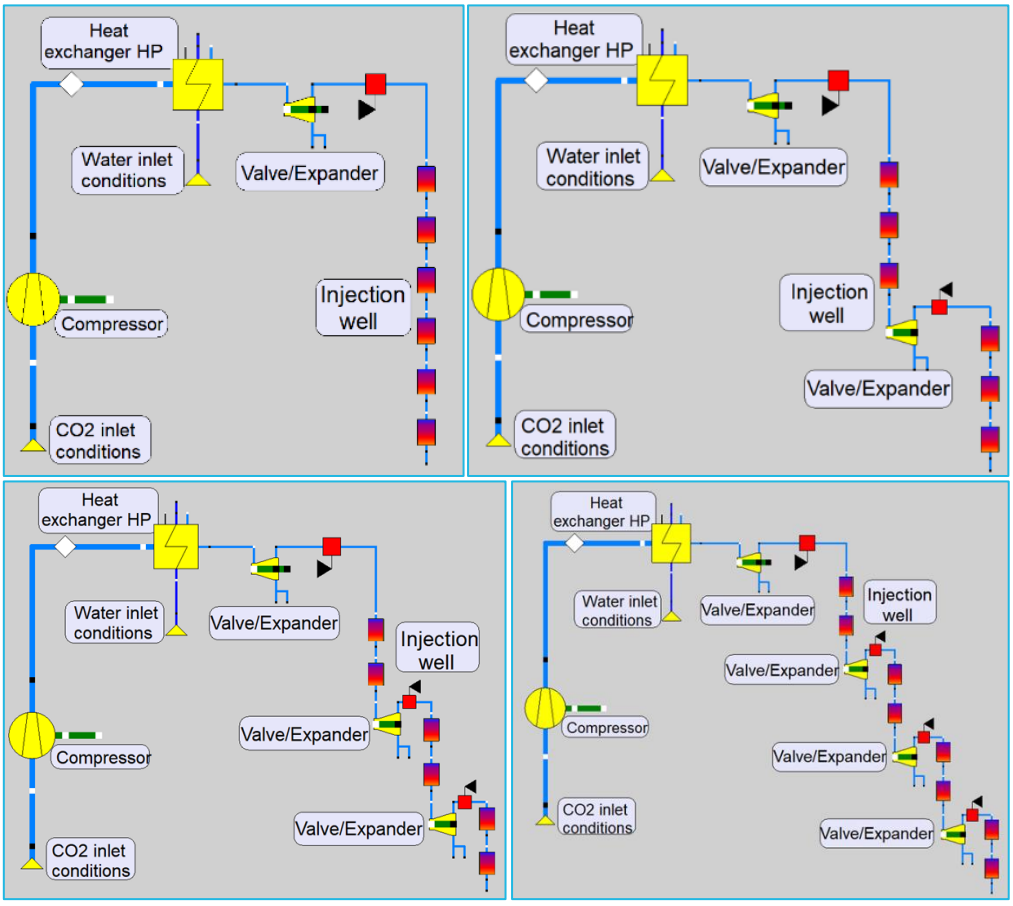

Figure 11. Ebsilon model. Conceptual scheme of the CEEGS system incorporating electrothermal energy storage and CO_2 geological storage.

During the modelling of the discharge phase operating in an open cycle, the following aspects have been taken into account in the CO_2 conditions in the discharge pipeline (both suction and outlet):

- Possible damage to the well casing due to a phase change within the well.
- Limited range of wellbore diameters below 0.5 m.
- Equilibrium conditions of the CO_2 stored in the plume are 70 ºC (ground temperature at 1800 m depth, with a gradient of 30 ºC/km) and 90 bar.

Table 6. Main assumptions made in the analysis of well piping

Length (total)	1800	m
Thickness	0.05	m
Pipe density	7850	kg/m3
Specific heat of pipe material	0.477	kJ/kg-K
Insulation thickness	0	M
Internal heat transfer coefficient	500	W/m²-K
External heat transfer coefficient	40	W/m²-K
Thermal gradient of the ground	30	ºC/km

4.5 Preliminary design of heat exchangers

A model in ASPEN was also developed with the ASPEN HYSYS and ASPEN EDR modules. It allows a detailed analysis of the components and heat exchanges, with predesigns for the heat exchangers of the system. The following assumptions have been made in the model:

- The head losses in the exchangers are assumed to be zero.
- The minimum temperature approach of the exchangers is considered to be 5 ºC.
- The work of the hydraulic turbine is neglected and replaced by a valve.
- R-22 is used as the fluid in LT-TES with a phase change approaching 0 ºC.

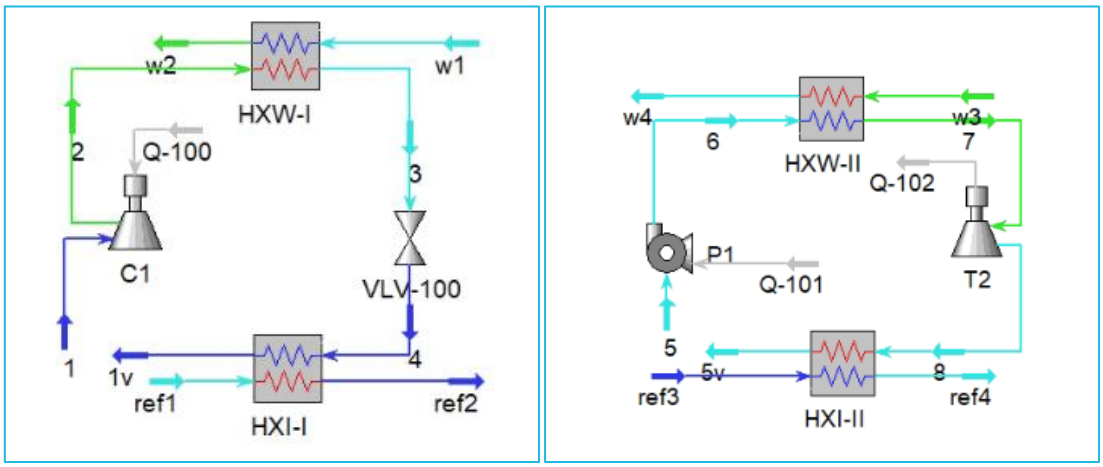

Figure 12. Aspen model. Conceptual scheme of the CEEGS system incorporating electrothermal energy storage

Heat exchangers design

Thermal and mechanical stresses depend on pressure, temperature differences and sizing. A preliminary qualitative selection of the heat exchanger type suitable for the CEEGS application was considered at this stage. Approaches to different typologies will be made in the next iterative analyses. Shell and tube heat exchangers are characterized by their versatility, wide range of temperatures, and allowable pressure for medium and high power. For moderate thermal power, the double tube

exchanger can work from vacuum to very high pressures, generally limited to 300 bar on the shell and 1400 bar on the tube side. For CEEGS conditions with liquid-liquid and liquid-phase-change exchangers and moderate temperatures and pressures (below 25 bar and 200 ºC), welded or gasketed plate heat exchangers should be considered. With higher pressures, fully welded or brazed plate heat exchangers should considered. The extended surface plate and fin heat exchanger can be used for low-pressure applications (< 10 bar). The maximum operating temperature of plate heat exchangers is below 650 ºC, generally less than 150 ºC.

Table 7. Types of exchangers considered and operating conditions

Type	Temp. Range (ºC)	Max. Pressure (bar)	Limitations Fluids	Cleaning Method	Corrosion resistance	Main limitation	Main advantage
Air coolant		500	-	-	Good		-
Welded plates	-35-200	40	Few	Chemistry	Material function	Corrosive fluids	-
Plates	-25-175	25	Gasket material	Mechanics and chemistry	Gaskets t plate	Pressures/Corrosive fluids/High temp	Inexpensive, low commuting
Double tube	-100-600	Shell 300 Tubes 1400	Few	Mechanics and chemistry	Material function	Power to transfer	Competitive for low areas
Housing and tube	-100-600	Shell 300 Tubes 1400	Few	Mechanics and chemistry	Seals t plate	Space	High power and robust
Spiral		30	Few	Mechanics	Good	Main limitation	High U, clean

In the case of transcritical CO_2 cycles, with maximum temperatures around 180 °C on the high-temperature side, pressures up to 240 bar, **shell and tube heat exchangers** can be adjusted to the operating requirements. They can withstand up to 300 bar in the shell, have a wide temperature range (-100 to 600 ºC), and operate at high power (12 to 30 MWth).

The selection of the location of each fluid would be conditioned by transfer, fouling and cleanability, pressure, corrosion and materials. The fluid located inside the tubes:

- It would be the one with the highest fouling for simplifying maintenance.
- The stream with higher pressure. It reduces the higher capital costs linked to high-pressure casings.
- The stream with higher corrosion potential.
- The one that requires special materials to avoid more expensive casings.

Table 8. Criteria for selecting the location of fluids in heat exchanges

Factor	Fluid Tubes	Casing fluid
Fouling	Dirtier	Less dirty
Corrosion	More corrosive	Less corrosive
Viscosity	Less viscous	More viscous
Pressure	High	Low
Temperature	High	Low
Pressure drop	Low	High
Flow rate	High flow rate	Low flow

In the case of CO_2 transcritical cycles, with a pressure range of 240 to 30 bar for CO_2, and ice and water conditions, with pressures close to atmospheric, CO_2 would be the selected fluid inside the tubes.

Although the fouling of water and R-22 would be higher than that of CO_2, the pressure restriction is imposed. The design distinguishes between the distribution head, the housing and the sealing head, with different types of each element varying according to their application.

The distribution header is stationary, while the rear or distribution header can be stationary or floating depending on the thermal stresses allowed between the pipes and the casing. The main criteria for selecting closure and distribution heads are thermal stresses, operating pressures, ease of cleaning, risks and cost.

Table 9. Proposed typologies for the different exchangers

Exchanger	Max ΔT (ºC)	Max Pressure (bar)	Distribution head	Housing	Shut-off head	Differential thermal expansion
HXW-I	156,6	240	D	E	U, T, S, P y W	*Yes*
HXW-II	130	240	D	E	U, T, S, P y W	*Yes*
HXI-I	4,04	30	C, D	E	U, T, S, P y W	No
HXI-II	17,51	40	C, D	E	U, T, S, P y W	No

According to the Tubular Exchanger Manufacturers Association (TEMA) standard [24], the D head has special high-pressure seals, being adequate for high-pressure applications (> 69 bar). They are selected for exchanges on the high-pressure side, where CO_2 pressures up to 240 bar can be reached. W as the sealing head is selected due to the thermal and mechanical stresses. The four heat exchangers analysed will be exposed to high pressures (>20 bar). HXI-I and HXI-II will have a differential thermal expansion, which further justifies the use of floating heads, especially the W, because of its lower cost.

5. CEEGS system. Numerical results of the models– Technical Analysis

5.1 Closed CO_2 transcritical cycles

The pressure range on the high-temperature side varies from 80 bar (a value somewhat higher than the critical pressure to maintain the characteristics of the transcritical cycles) to 240 bar. Figure 13a shows on the CO_2 T-s diagram, the transcritical processes for a pressure of 240 bar in the charging phase (1-2-3-4) and 80 bar in the discharging step (5-6-7-8) and the temperature lines corresponding to the HT-TES in red and LT-TES in blue. Figure 13b shows the T-Q diagram of the high-temperature exchangers in charging and discharging, representing the excellent integration of the temperature profile and the temperature difference between the two exchangers. Temperature differences between the HTF (CO_2) and the stored material are indicated for both the charging and discharging stages.

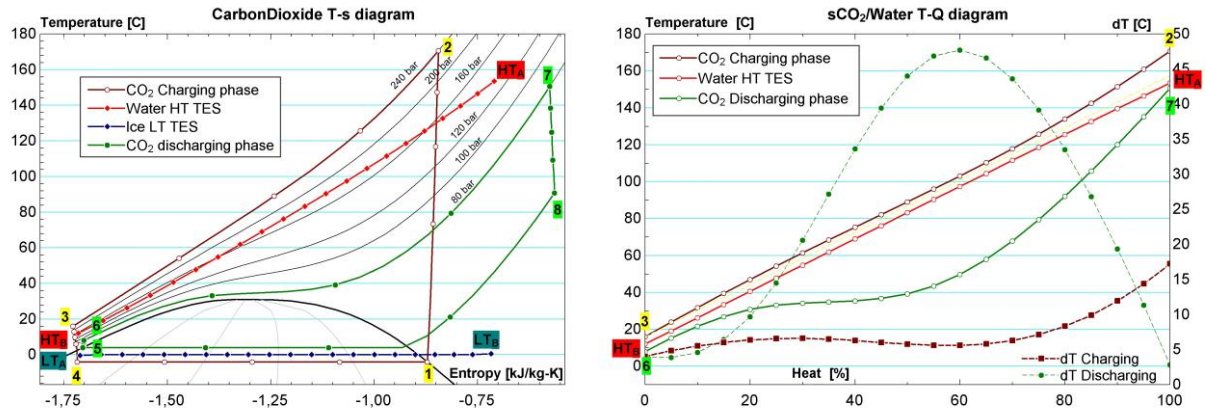

a) b)

Figure 13. a) T-s diagram of CO_2 representing the transcritical cycles of charging and discharging and thermal storage, and b) T-Q diagram of the heat exchanges on the high-temperature side, considering CO_2 pressures of 240 bar in the charging phase and 80 bar in the discharging phase.

A study of how the variation in pressure values in the high zone affects the system's characteristics is carried out. For this purpose, a parametric analysis is performed in the pressure range of 80-240 bar, considering increments of 20 bar. The whole high-pressure range in the discharging phase is assessed for each high-pressure value in the charging stage. Figure 14 shows the CO_2 T-s diagram, in which the charging and discharging cycles of the TEES system are represented for a fixed high pressure in the charging phase of 200 bar (left) and 240 bar (right), and the whole range of analysis in the discharging high pressure.

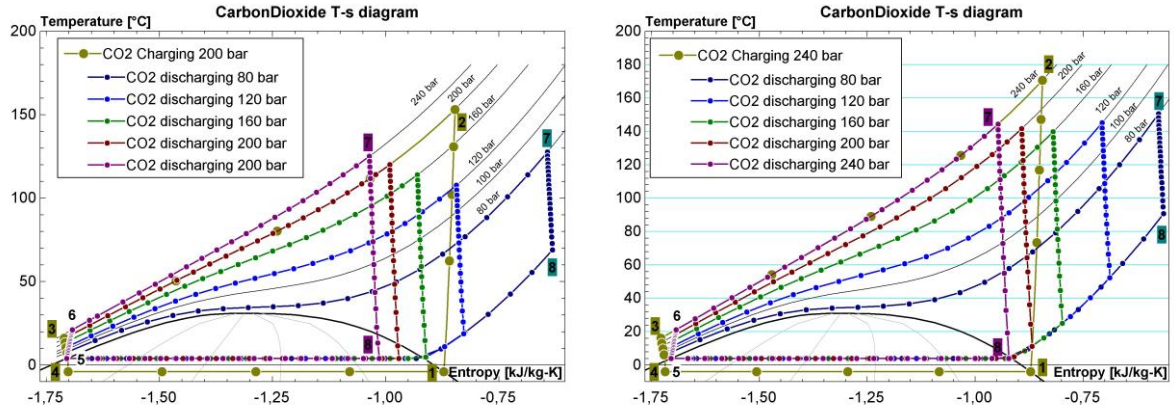

Figure 14. Variation of the shape of CO_2 transcritical cycles in the T-s diagram, in which the pressure of the high-temperature side of the charging phase is constant and that of the discharging stage varies in the range of 80-240 bar, considering a CO_2 pressure at the charging of: a) 200 bar; b) 240 bar.

From the CO_2 T-s diagrams, some details can be seen at a glance, such as the higher the pressure in the charging phase (240 bar on the right and 200 bar on the left), the higher the compressor outlet temperature (Point 2) and the higher the turbine inlet temperature (Point 7), increasing the available turbine head. For the discharging phase cycles, the turbine expansion line (7-8) establishes different trends: when the discharging pressure is above the charging pressure, this expansion line enters the two-phase zone, while when it is below, it moves to the right, decreasing the available enthalpy jump due to the shape of the constant pressure curve. The shape of the cycles in the diagram suggests that the best results will be obtained at close pressure values. A slight improvement is obtained when the discharging pressure is somewhat lower than the charging pressure due to the small shift to the right introduced by the influence of the isentropic performance of the equipment. In addition, at higher

pressure values, a higher temperature is achieved at the turbine inlet, increasing the available enthalpy gain.

Table 10 shows the results of some variables for the complete parametric analysis. Each simulation performed shows, from left to right and from top to bottom, the roundtrip efficiency of the TEES system, considering the complete discharging of the hot water tank (1) and the complete discharging of the ice tank (2), the high temperature (ºC) in the high-temperature TES storage (3) and the temperature (ºC) of the gas turbine inlet (4) in the discharging phase.

Table 10. Parametric analysis results by modifying the pressure values of the high-temperature side.

(1)	(2)	Discharging phase - CO_2 high Pressure (bar)													
(3)	(4)	240		220		200		180		160		120		80	
Charging Phase - CO_2 high pressure	240	0.578	0.490	0.565	0.480	0.549	0.466	0.535	0.457	0.494	0.420	0.368	0.312	-	-
		156.3	144.4	147.6	135.1	137.9	125.1	127.1	116.6	114.9	102.8	84.8	76.4	-	-
	220	0.577	0.489	0.565	0.481	0.546	0.465	0.527	0.450	0.500	0.427	0.389	0.332	-	-
		156.4	142.4	147.7	133.2	138.0	122.2	127.3	112.1	115.2	101.0	85.2	75.6	-	-
	200	0.577	0.490	0.563	0.479	0.546	0.466	0.526	0.449	0.504	0.431	0.405	0.347	-	-
		156.6	141.8	147.8	130.9	138.2	120.1	127.5	109.2	115.4	98.7	85.5	74.1	-	-
	180	0.567	0.481	0.556	0.473	0.542	0.462	0.521	0.445	0.500	0.428	0.416	0.359	-	-
		156.6	139.0	147.9	128.1	138.3	117.4	127.6	105.6	115.6	95.0	85.8	72.0	-	-
	160	0.559	0.473	0.548	0.465	0.533	0.454	0.515	0.440	0.495	0.425	0.424	0.366	0.054	0.046
		156.8	139.9	148.1	126.5	138.5	114.1	127.8	102.3	115.8	91.1	86.2	69.2	43.9	38.3
	120	0.508	0.425	0.503	0.423	0.491	0.414	0.474	0.401	0.455	0.387	0.413	0.358	0.204	0.178
		156.2	145.2	147.9	126.5	138.7	107.9	128.1	91.9	116.2	78.7	86.8	59.0	45.3	37.5
	80	0.370	0.297	0.378	0.307	0.385	0.316	0.368	0.303	0.348	0.289	0.335	0.286	0.247	0.217
		153.4	150.6	144.5	141.4	134.8	127.6	124.1	84.8	112.5	60.4	87.5	38.7	46.5	31.2

(1) Global efficiency (equation 3) considering the hours in the discharge phase to achieve complete discharge of the hot water tank
(2) Global efficiency (equation 3) considering the hours in the discharge phase to achieve complete discharge of the ice tank
(3) Temperature of the HT-TES hot water tank
(4) Temperature of the discharging phase turbine inlet

The most relevant information that can be extracted from Table 10 is the difference in the value of the system's roundtrip efficiency if the discharging hours of HT-TES (hot water) or LT-TES (ice) are considered. It shows that the system does not have a balanced discharging, i.e., when the discharging phase is carried out, one of the two tanks, in this analysis, the one corresponding to LT-TES, is "empty" or wholly discharged before the other one. This difference establishes a "minimum" roundtrip efficiency, marked by the discharging of the LT-TES, in which a surplus of thermal energy would remain unused in the HT-TES, and a maximum roundtrip efficiency, marked by the discharging of the HT-TES, which would require additional energy input in the LT-TES.

This maximum achievable roundtrip efficiency is plotted in Figure 15. It plots the efficiency versus the difference between the high pressures of the charging and discharging phases. Positive values correspond to charging pressures higher than the discharging pressure, while negative values correspond to discharging pressures above the charging pressure. Each analysis series is shown in a different colour with the charging pressure fixed, as the legend indicates.

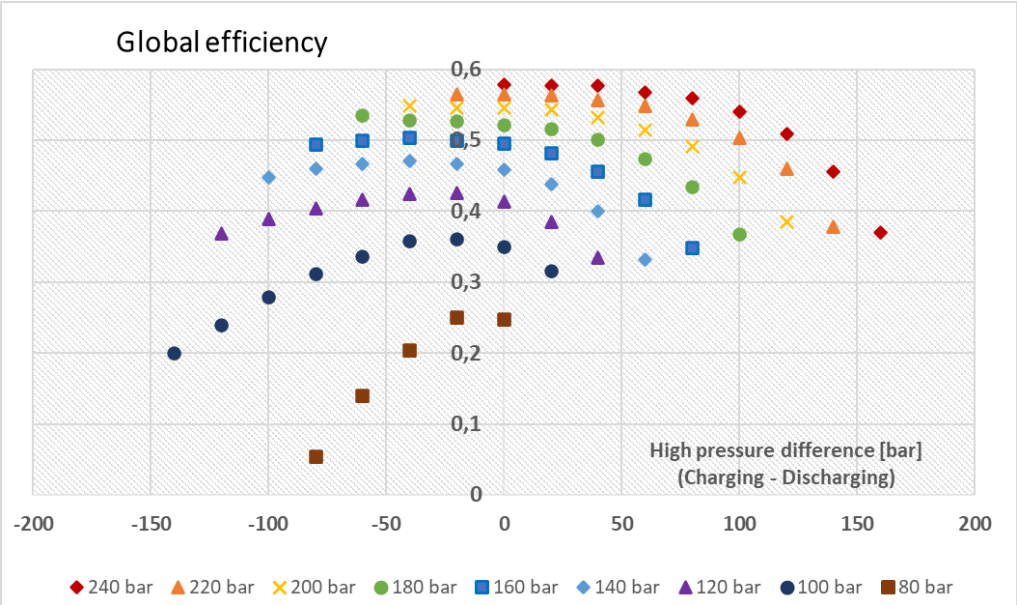

Figure 15. Round-trip efficiency considering HT-TES discharging hours versus the difference between charging and discharging pressures (bar) on the high-temperature side.

As was intuited in the shape of the cycles in the T-s diagram, the highest efficiency values occur as the high charging pressure increases and in the central zone, where the two pressures have values close to each other. It should be noted that some values of the last analysis (charging pressure of 80 bar) are out of the expected range. They correspond to very low-quality expansion lines within the two-phase zone, which leaves them out of consideration in this study.

The high-efficiency cases, above 50%, include all combinations of pressure on the high-temperature side of the charging and discharging phase above 160 bar, and some combinations for even higher pressures, such as the case of 140 bar in discharging for 180-240 bar in the charging phase and the case of 120 bar in discharging for 220-240 bar in the charging phase.

5.1.1 Charging phase.

The following figure shows the pressure-enthalpy (P-h) & temperature-entropy (T-s) diagrams (2d) and T-s (3d) diagram of the CO_2 transcritical cycle of the charging phase, considering a pressure range on the high-temperature side of 200-240 bar.

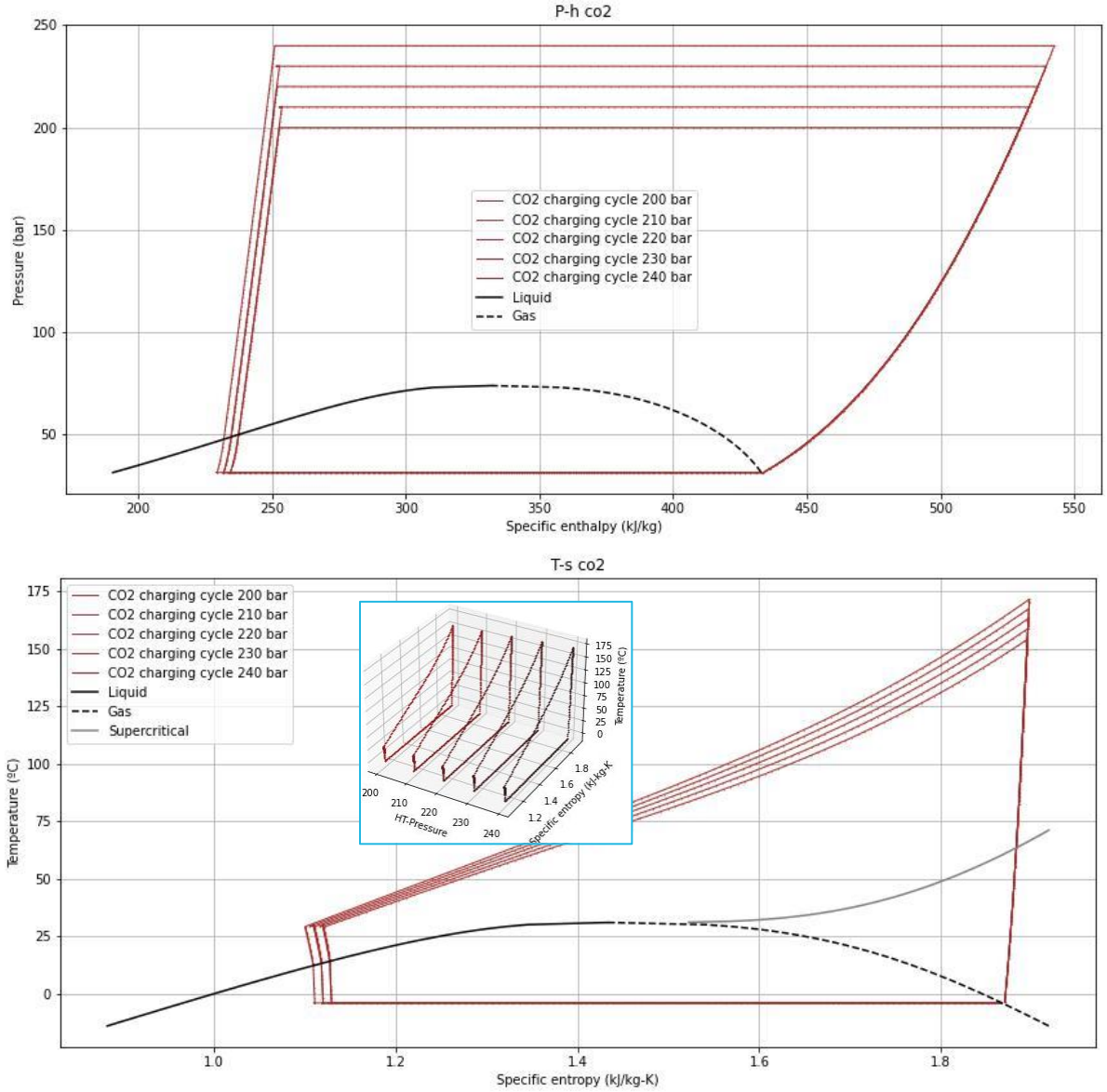

Figure 16. P-h (up) & T-s (down) (2d) and T-s (3d) diagrams of the CO_2 transcritical cycles for 240 bar in charging phase

A detailed analysis of the combination with the same range of pressures for the high-temperature side of the discharge phase (200-240 bar) is then performed for each charging pressure value on the high-temperature side.

5.1.2 High-temperature side charging pressure: 240 bar.

The following figure shows the P-h (2d) and T-s (3d) diagrams of the CO_2 transcritical cycles of the charging phase (240 bar), considering a pressure range on the high-temperature side of the discharge phase of 200-240 bar.

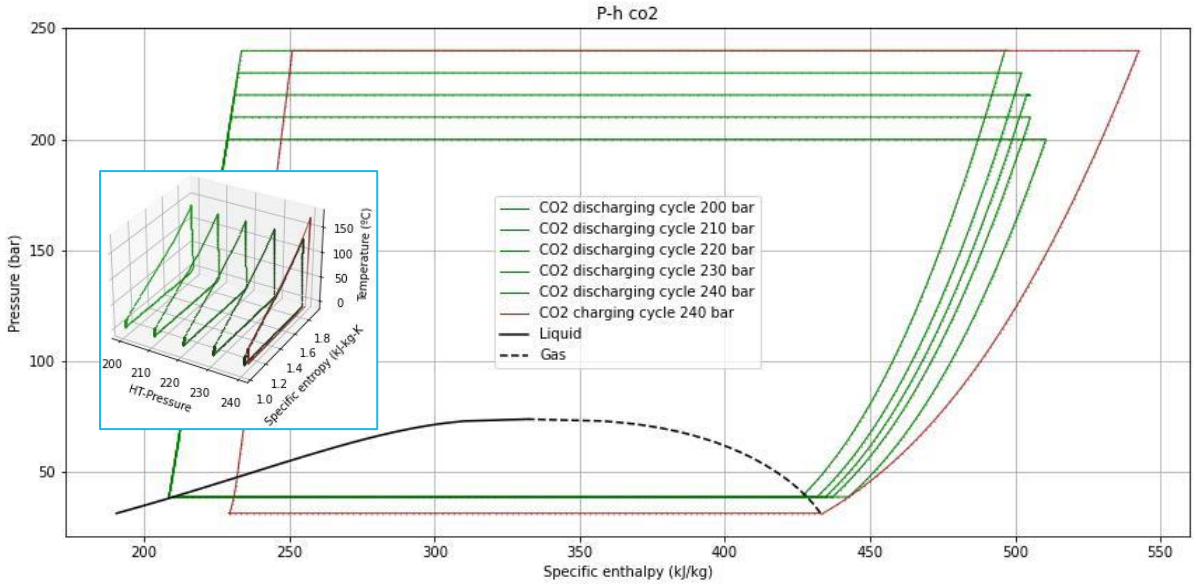

Figure 17. P-h (2d) and T-s (3d) diagrams of the CO_2 transcritical cycles for 240 bar in charging

Table 11. Round-trip efficiency considering 240 bar in charging HT-Pressure

(1)	Discharging phase - CO_2 high Pressure (bar)									
(2)	240		230		220		210		200	
240	57.7	48.8	57.6	49.1	**58.2**	**49.6**	58.1	49.2	57.8	49.3

(1) Global efficiency (equation 3) considering the hours in the discharge phase to achieve complete discharge of the hot water tank
(2) Global efficiency (equation 3) considering the hours in the discharge phase to achieve complete discharge of the ice tank

The maximum efficiency point occurs in the 240-220 bar combination in the charging and discharging phases, respectively, exceeding 58% in the round-trip efficiency considering the complete discharge of the HT tank. Considering the balanced discharge of both tanks, the system would reach 49.6%, leaving a surplus of energy in the high-temperature tank.

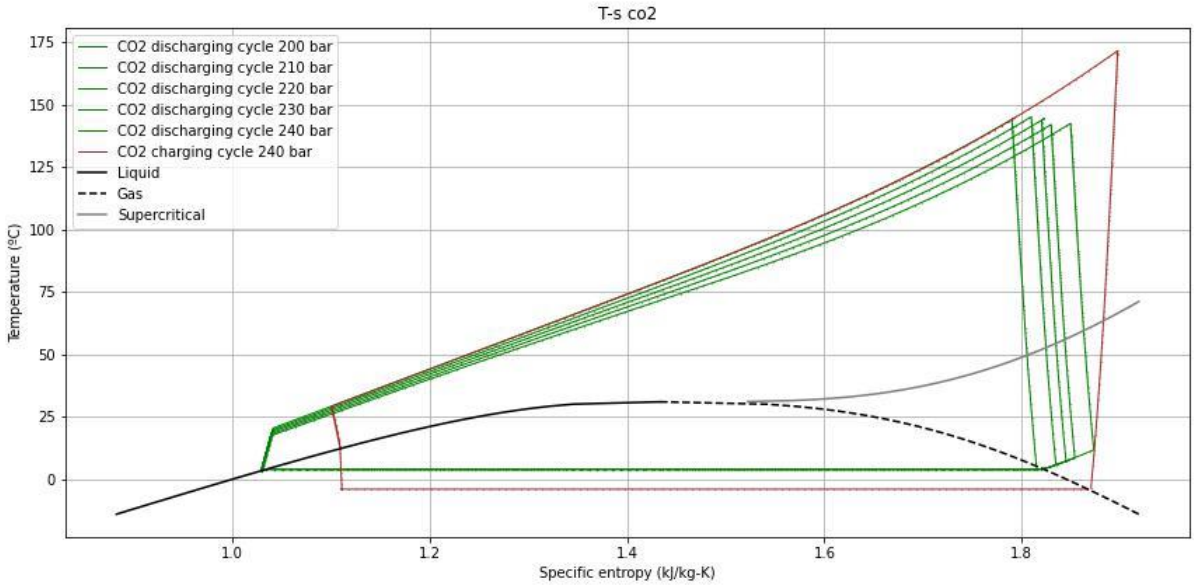

Figure 18. T-s diagrams of the charging phase [240 bar] and discharging phase [200-240 bar]

The thermodynamic properties of the CO_2 transcritical cycles for the charging (1-2-3-4) and discharging (5-6-7-8) phases in the case of maximum round-trip efficiency considering a discharging pressure of 220 bar on the high-temperature side are shown below.

Table 12. Cycle properties. HT-Pressures: 240 bar charging and 220 bar discharging

Ref	Pressure (bar)	Temp (°C)	Quality/State -	Enthalpy (kJ/kg)	Entropy (kJ/kgK)	Density (kg/m^3)
Charging cycle						
1	31.3	-4	1	432.95	1.87	86.02
2	240	170.7	sc	541.26	1.89	356.68
3	240	27.7	sc	248	1.09	926.4
4	31.3	-4	0.15	226.78	1.1	379.1
Discharging cycle						
5	38.69	4	0	209.95	1.03	902.55
6	220	19.7	sc	232.51	1.05	949.36
7	220	144.39	sc	505.07	1.82	376.04
8	38.69	7.6	steam	435.26	1.85	105.64

5.1.3 High-temperature side charging pressure: 230 bar.

The following figure shows the P-h (2d) and T-s (3d) diagrams of the CO_2 transcritical cycles of the charging phase (230 bar), considering a pressure range on the high-temperature side of the discharge phase of 200-240 bar.

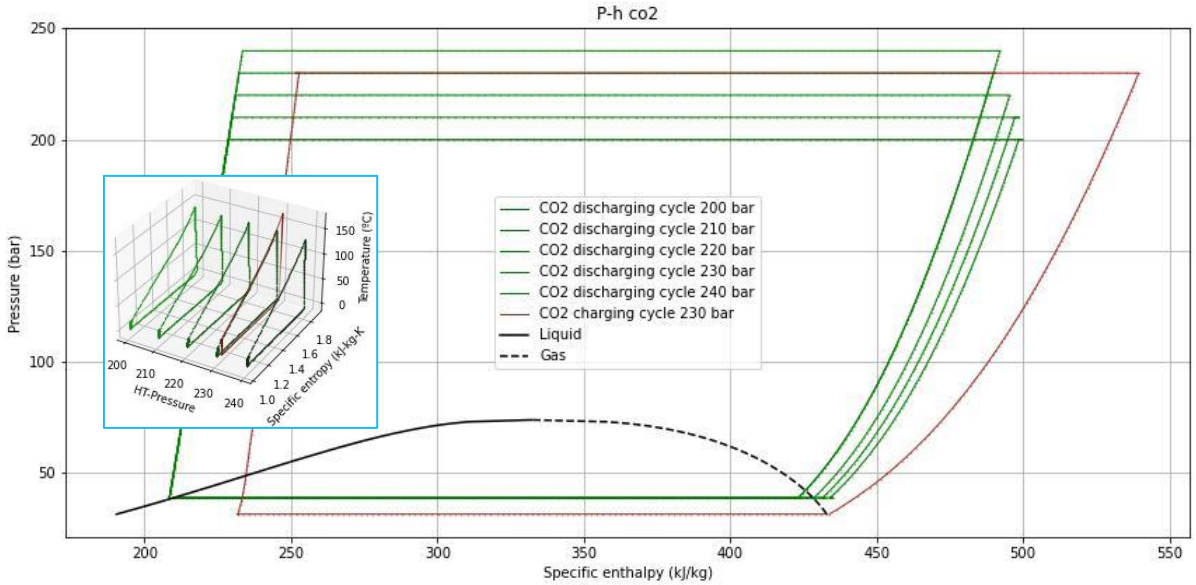

Figure 19. P-h (2d) and T-s (3d) diagrams of the CO_2 transcritical cycles for 230 bar in charging

Table 13. Round-trip efficiency considering 230 bar in charging HT-Pressure

(1)	Discharging phase - CO_2 high Pressure (bar)									
(2)	240		230		220		210		**200**	
230	57.0	48.6	57.4	48.9	57.3	48.8	57.2	48.5	**57.5**	**48.8**

(1) Global efficiency (equation 3) considering the hours in the discharge phase to achieve complete discharge of the hot water tank
(2) Global efficiency (equation 3) considering the hours in the discharge phase to achieve complete discharge of the ice tank

The maximum efficiency point occurs in the 230-200 bar combination in the charging and discharging phases, respectively, exceeding 57% in the round-trip efficiency considering the complete discharge of the HT-tank. Considering the balanced discharge of both tanks, the system would reach 48.8%, leaving a surplus of energy in the high-temperature tank. Figure 20 shows the P-h (top) and T-s (bottom) diagrams for the maximum efficiency case.

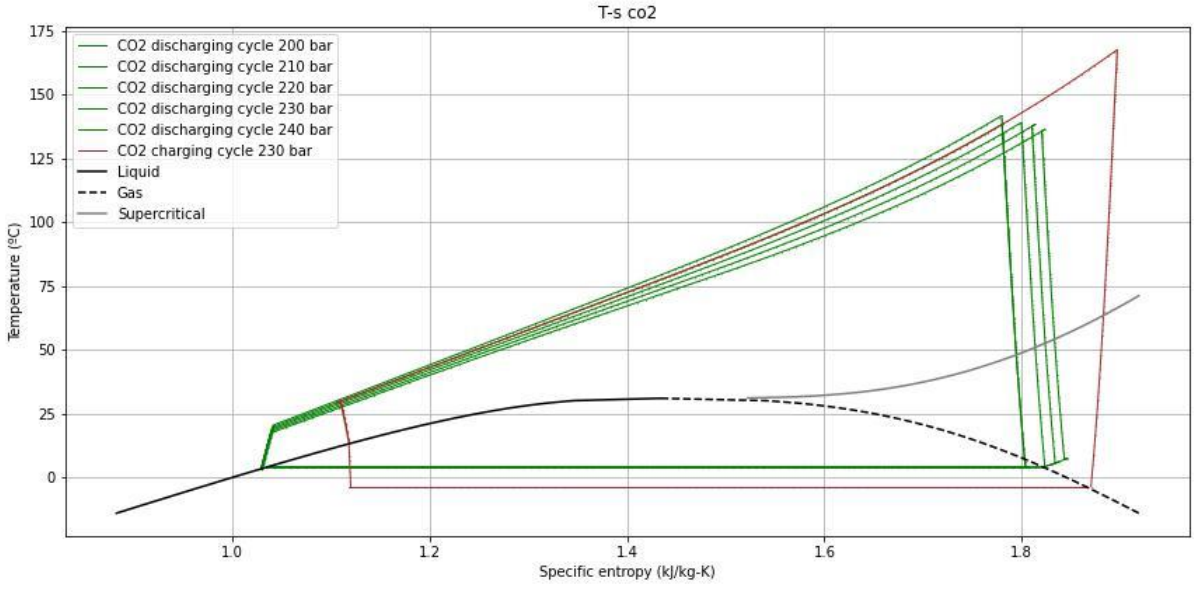

Figure 21. T-s diagrams of the charging phase [230 bar] and discharging phase [200-240 bar]

The thermodynamic properties of the CO_2 transcritical cycles for the charging (1-2-3-4) and discharging (5-6-7-8) phases in the case of maximum round-trip efficiency considering a discharging pressure of 200 bar on the high-temperature side are shown below.

Table 14, Cycle properties. HT-Pressures: 200 bar charging and discharging values

Ref	Pressure (bar)	Temp (°C)	Quality/State -	Enthalpy (kJ/kg)	Entropy (kJ/kgK)	Density (kg/m^3)
Charging cycle						
1	31.3	-4	1	432.95	1.87	86.02
2	230	166.6	sc	538.17	1.89	348.26
3	230	26.2	sc	245.36	1.09	927.11
4	31.3	-4	0.14	224.35	1.09	394.93
Discharging cycle						
5	38.69	4	0	209.95	1.03	902.55
6	200	18.2	sc	230.15	1.04	945.04
7	200	136.29	sc	499.86	1.82	356.09
8	38.69	7.5	Steam	435.08	1.85	105.78

5.1.4 High-temperature side charging pressure: 220 bar

The following figure shows the P-h (2d) and T-s (3d) diagrams of the CO_2 transcritical cycles of the charging phase (220 bar), considering a pressure range on the high-temperature side of the discharge phase of 200-240 bar.

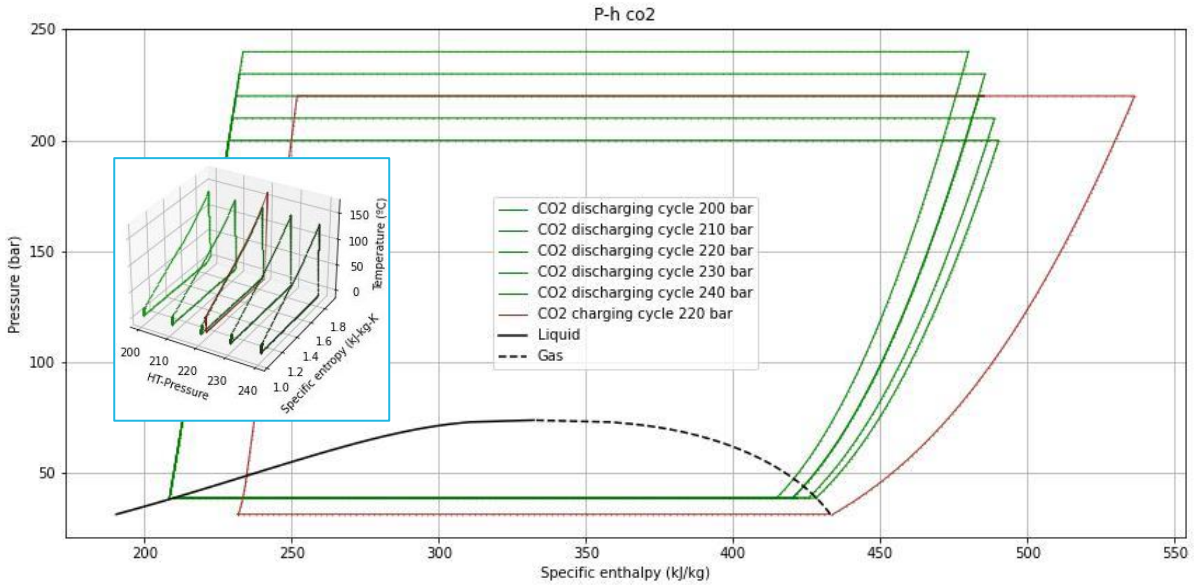

Figure 22. P-h (2d) and T-s (3d) diagrams of the CO_2 transcritical cycles for 220 bar in charging

Table 15. Round-trip efficiency considering 220 bar in charging HT-Pressure

(1)	Discharging phase - CO_2 high Pressure (bar)									
(2)	240		230		220		**210**		200	
220	56.2	47.5	56.6	48.7	56.6	48.1	**56.9**	**48.2**	56.6	48.0

(1) Global efficiency (equation 3) considering the hours in the discharge phase to achieve complete discharge of the hot water tank
(2) Global efficiency (equation 3) considering the hours in the discharge phase to achieve complete discharge of the ice tank

In this case, the efficiency presents a relatively flat zone around 56-57%, placing the point of maximum efficiency in the 220-210 bar combination in the charging and discharging phases, respectively, almost reaching 57% in the round-trip efficiency considering the complete discharge of the tank at high. Due to the balanced discharge of both tanks, the system will reach 49.2%, leaving a surplus of energy in the high-temperature tank, although it presents a better LT-efficiency for 220-230 bar, where it stands at 48.7%. The following figure shows the P-h (top) and T-s (bottom) diagrams for the 220-210 bar case.

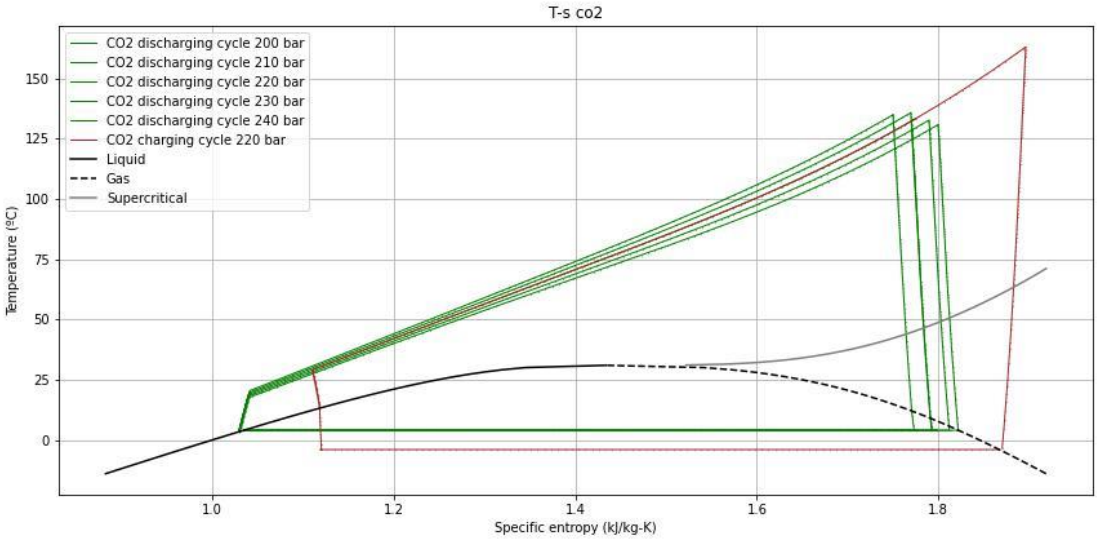

Figure 23. T-s diagrams of charging phase [220 bar] and discharging phase [200-240 bar]

The thermodynamic properties of the CO_2 transcritical cycles for the charging (1-2-3-4) and discharging (5-6-7-8) phases in the case of maximum round-trip efficiency considering a discharging pressure of 210 bar on the high-temperature side, are shown below.

Table 16, Cycle properties. HT-Pressures: 220 bar charging and 210 bar discharging

Ref	Pressure (bar)	Temp (°C)	Quality/State -	Enthalpy (kJ/kg)	Entropy (kJ/kgK)	Density (kg/m^3)
Charging cycle						
1	31.3	-4	1	432.95	1.87	86.02
2	220	162.3	sc	534.96	1.89	339.6
3	220	26.2	sc	245.81	1.09	921.25
4	31.3	-4	0.15	226.78	1.1	379.1
Discharging cycle						
5	38.69	4	0	209.95	1.03	902.55
6	210	19	sc	231.42	1.05	947.02
7	210	132.37	sc	487.97	1.79	386.56
8	38.69	4	0.98	423.88	1.81	112.96

5.1.5 High-temperature side charging pressure: 210 bar

The following figure shows the P-h (2d) and T-s (3d) diagrams of the CO_2 transcritical cycles of the charging phase (210 bar), considering a pressure range on the high-temperature side of the discharge phase of 200-240 bar.

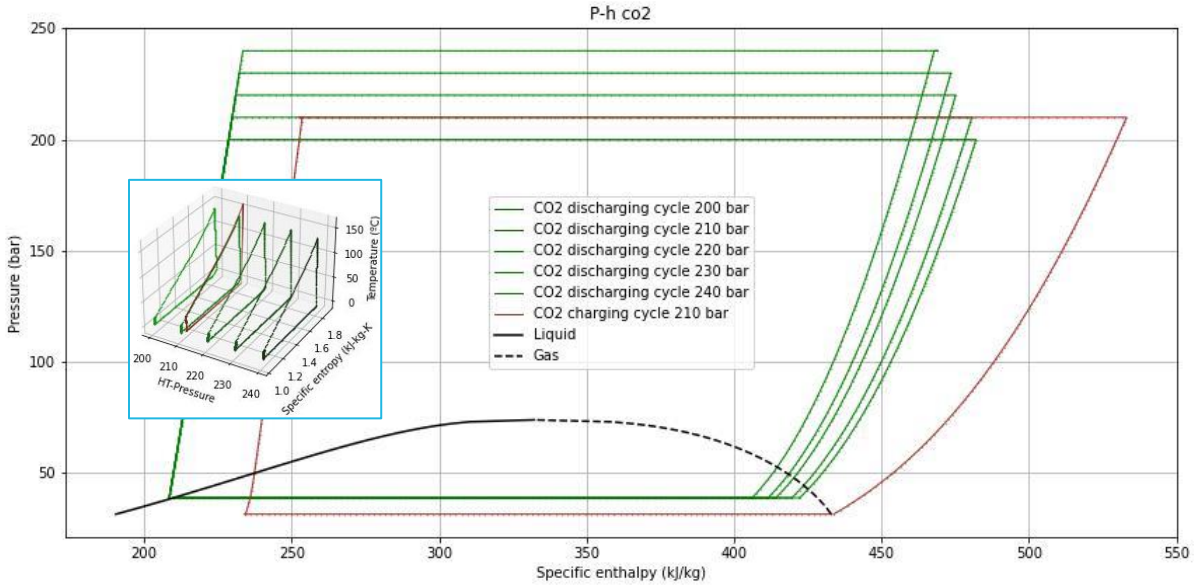

Figure 24. P-h (2d) and T-s (3d) diagrams of the CO_2 transcritical cycles for 210 bar in charging

Table 17. Round-trip efficiency considering 210 bar in charging HT-Pressure

(1)	Discharging phase - CO_2 high Pressure (bar)									
(2)	240		230		220		**210**		200	
210	55.6	47.5	55.8	47.4	55.7	47.4	**55.9**	**47.8**	55.4	47.2

(1) Global efficiency (equation 3) considering the hours in the discharge phase to achieve complete discharge of the hot water tank
(2) Global efficiency (equation 3) considering the hours in the discharge phase to achieve complete discharge of the ice tank

In this case, the efficiency presents a relatively flat region around 55.5-56%, the maximum efficiency point being located in the 210-210 bar combination in the charging and discharging phases, respectively, reaching almost 56% in the round-trip efficiency considering the complete discharge of the tank at high. The system will reach 47.8%, leaving a surplus of energy in the high-temperature tank. The following figure shows the P-h (top) and T-s (bottom) diagrams for the 210-210 bar case.

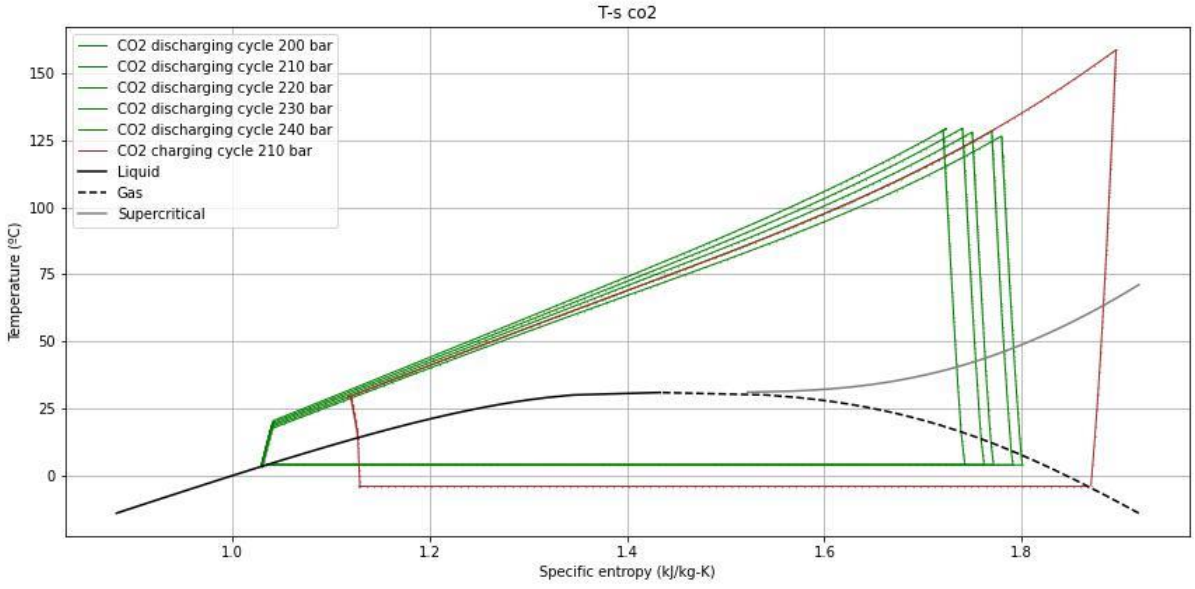

Figure 25. T-s diagrams of the charging phase [210 bar] and discharging phase [200-240 bar]

The thermodynamic properties of the CO_2 transcritical cycles for the charging (1-2-3-4) and discharging (5-6-7-8) phases in the case of maximum round-trip efficiency considering a discharging pressure of 210 bar on the high-temperature side are shown below.

Table 18, Cycle properties. HT-Pressures: 210 bar charging and discharging

Ref	Pressure (bar)	Temp (°C)	Quality/State -	Enthalpy (kJ/kg)	Entropy (kJ/kgK)	Density (kg/m^3)
Charging cycle						
1	31.3	-4	1	432.95	1.87	86.02
2	210	157.9	sc	531.8	1.89	330.48
3	210	26.2	sc	246.31	1.1	915.1
4	31.3	-4	0.15	226.78	1.1	379.1
Discharging cycle						
5	38.69	4	0	209.95	1.03	902.55
6	210	19	sc	231.42	1.05	947.02
7	210	127.55	sc	478.93	1.77	400.13
8	38.69	4	0.96	419.52	1.79	115.02

5.1.6 High-temperature side charging pressure: 200 bar

The following figure shows the P-h (2d) and T-s (3d) diagrams of the CO_2 transcritical cycles of the charging phase (210 bar), considering a pressure range on the high-temperature side of the discharge phase of 200-240 bar.

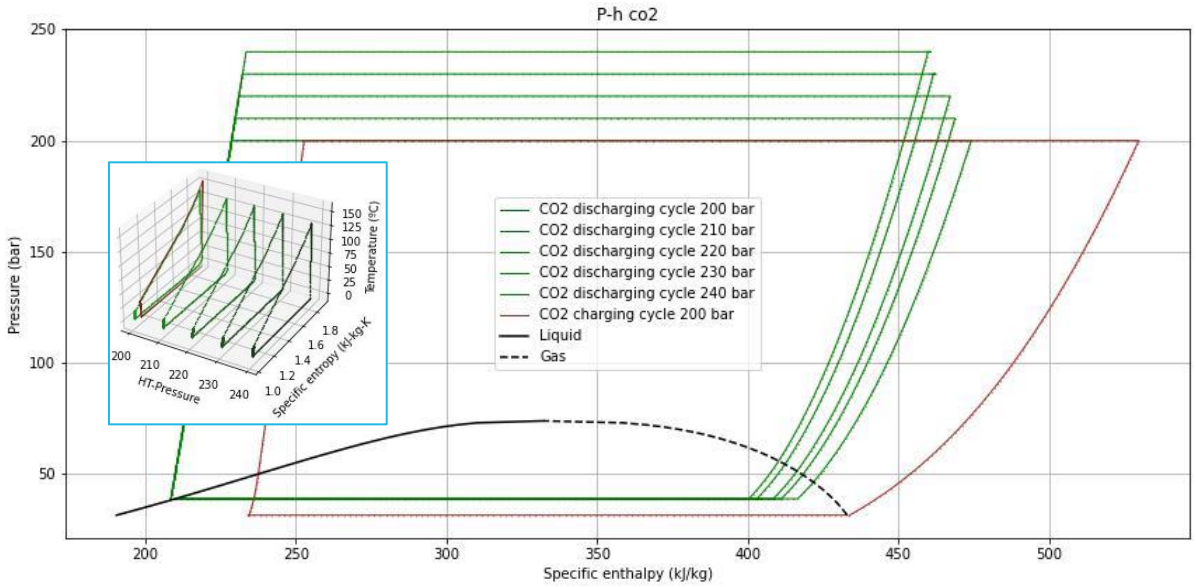

Figure 26. P-h (2d) and T-s (3d) diagrams of the CO_2 transcritical cycles for 200 bar in charging

Table 19. Round-trip efficiency considering 200 bar in charging HT-Pressure

(1)	Discharging phase - CO_2 high Pressure (bar)									
(2)	**240**		230		220		210		200	
200	**55.2**	**47.2**	54.8	46.6	55.1	46.9	54.8	46.2	54.8	47.0

(1) Global efficiency (equation 3) considering the hours in the discharge phase to achieve complete discharge of the hot water tank
(2) Global efficiency (equation 3) considering the hours in the discharge phase to achieve complete discharge of the ice tank

The maximum efficiency point occurs in the 200-240 bar combination in the charging and discharging phases, respectively, exceeding 55% in the round-trip efficiency considering the complete discharge of the HT-tank. Considering the balanced discharge of both tanks, the system will reach 47.2%, leaving a surplus of energy in the high-temperature tank.

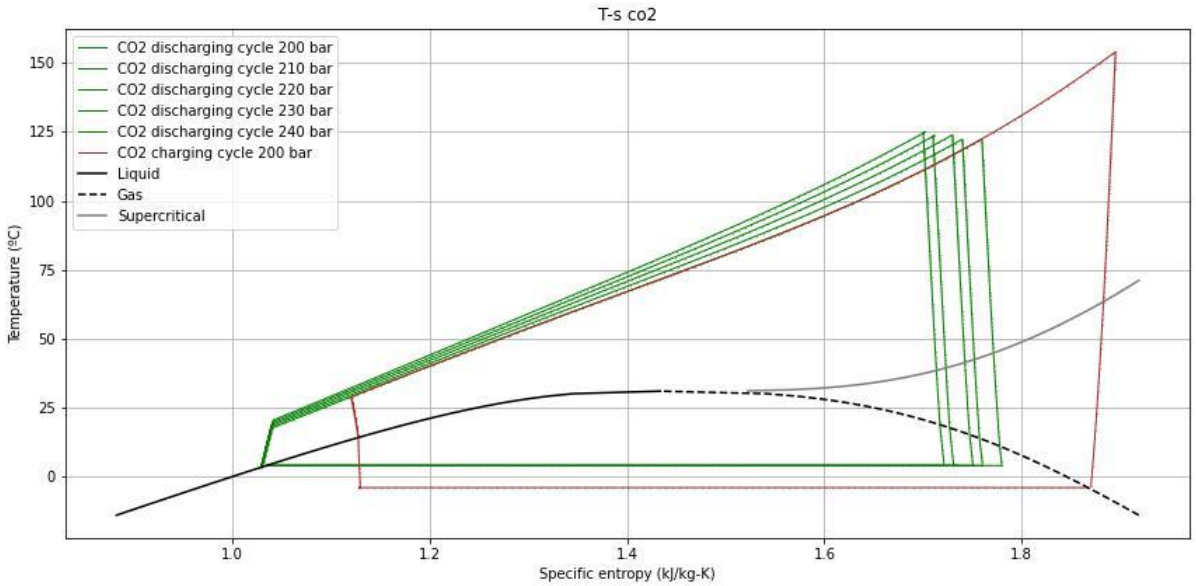

Figure 27. T-s diagrams of the charging phase [200 bar] and discharging phase [200-240 bar]

The thermodynamic properties of the CO_2 transcritical cycles for the charging (1-2-3-4) and discharging (5-6-7-8) phases in the case of maximum round-trip efficiency considering a discharging pressure of 240 bar on the high-temperature side are shown below.

Table 20. Cycle properties. HT-Pressures: 200 bar charging and discharging

Ref	Pressure (bar)	Temp (ºC)	Quality/State -	Enthalpy (kJ/kg)	Entropy (kJ/kgK)	Density (kg/m^3)
Charging cycle						
1	31.3	-4	1	432.95	1.87	86.02
2	200	153.2	sc	528.4	1.89	321.21
3	200	29.2	sc	253.28	1.12	894.36
4	31.3	-4	0.18	234.05	1.13	338.41
Discharging cycle						
5	38.69	4	0	209.95	1.03	902.55
6	240	21.2	sc	234.94	1.05	953.37
7	240	125.01	sc	460.68	1.7	469.11
8	38.69	4	0.87	399.87	1.72	125.26

5.2 Sizing of the storage plant

After studying the impact of the values of CO_2 pressures on the high-temperature side, this section is devoted to analysing the differences in the TEES-CO_2 system when considering two different plant sizes: 5 MW and 100 MW. The following analyses show the study selecting a value of 200 bar for the CO_2 high pressure in both the charging and discharging phases. A preliminary analysis considers a 10-hour charging phase with a constant electrical power input (the plant size is considered the same in both the charging and discharging phases, i.e. the net electrical power consumed in the charging stage is equal to the output in the discharging phase). The main results are shown in Table 21.

Table 21. Preliminary sizing of the storage plant as a function of net capacity

Size	Net power (In/Out)	MW_e	5	100
Transcritical CO_2 cycle	Charging flow rate	kg/s	64.3	1286
	Discharging flow rate	kg/s	138.4	2769
TES-HT	Volume	m^3	1439	28790
	Thermal power – discharging	MW_{th}	33.14	662.84
	Discharging hours	h	5.46	5.46
TES-LT	Volume	m^3	1531	30627
	Thermal power - discharging	MW_{th}	28.14	562.83
	Discharging hours	h	4.66	4.66

The size of the equipment is directly proportional to the net electrical power in each phase. The thermodynamic cycle remains unchanged, regarding the pressure values and design criteria. Table 21 includes the hours of discharging available in each tank (HT-TES and LT-TES). These discharging hours directly relate to the "maximum" and "minimum" roundtrip efficiency. Once the period established by the discharge hours of the LT-TES (lowest value in this case) is reached, the system cannot continue operating without an external energy input to balance the discharging. In other words, there always comes a time when the ice tank (in this case) is "empty" while the water tank still has a surplus (17.31%).

A more detailed analysis is shown below. First, the results of the mass and power balance of the charging and discharging (Table 22) phases are shown for a wider range of net electrical power in each phase (1-100 MWe). Details of mass flow and power for the complete CO_2 cycle are provided.

Table 22. *Power balance* of the *charging* as a function of net capacity

Power in (MW)	CO_2 flow rate (kg/s)	Compressor (MW)	Hydraulic (MW)	HT-hx (MW)	LT-hx (MW)	Water Flow rate (kg/s)	Ice Flow rate* (kg/s)
1	12.86	-1.23	0.23	3.62	-2.62	7.29	7.85
5	64.29	-6.14	1.14	18.1	-13.1	36.46	39.27
10	128.58	-12.28	2.28	36.2	-26.2	72.91	78.55
50	642.92	-61.39	11.39	180.99	-130.99	364.55	392.71
100	1285.84	-122.78	22.79	361.99	-261.99	729.11	785.46
Power out (MW)	**CO_2 flow rate (kg/s)**	**Pump (MW)**	**Turbine (MW)**	**HT-hx (MW)**	**LT-hx (MW)**	**Water Flow rate (kg/s)**	**Ice Flow rate* (kg/s)**
1	27.05	-0.55	1.55	-6.56	5.55	13.21	16.64
5	135.24	-2.73	7.73	-32.8	27.75	66.07	83.2
10	270.49	-5.46	15.46	-65.61	55.5	132.15	166.39
50	1352.45	-27.32	77.32	-328.05	277.52	660.75	832.02
100	2704.9	-54.64	154.64	-656.1	555.05	1321.5	1664.07

* Equivalent ice mass flow

The energy balance is developed from the mass and power balance, considering charging and discharging periods of 1-10 hours. The cases for a 5 and 100 MW plant capacity are shown for the charging and discharging phases.

Table 23 shows the energy balance for the charging phase. The columns “Total mass”, – “Water” & “Ice” show the amount of water stored after the number of hours of operation considered for each power and the amount of ice needed to store the corresponding energy in each case, respectively.

Table 23. Energy balance of the charging phase as a function of net capacity

Power (MW)	Time(h)	Electrical energy (MWh)			Heat (MWh)		Total mass (t)	
Net	Charging	Net	Compressor	Hydraulic	HT-hx	LT-hx	Water	Ice
5	1	5	-6.14	1.14	18.1	-13.1	131.26	141.37
5	2	10	-12.28	2.28	36.2	-26.2	262.51	282.74
5	4	20	-24.56	4.56	72.4	-52.4	525.02	565.49
5	6	30	-36.84	6.84	108.6	-78.6	787.54	848.23
5	8	40	-49.12	9.12	144.8	-104.8	1050.05	1130.98
5	10	50	-61.4	11.4	181	-131	1312.56	1413.72
100	1	100	-122.78	22.79	361.99	-261.99	2624.8	2827.66
100	2	200	-245.56	45.58	723.98	-523.98	5249.59	5655.31
100	4	400	-491.12	91.16	1447.96	-1047.96	10499.18	11310.62
100	6	600	-736.68	136.74	2171.94	-1571.94	15748.78	16965.94
100	8	800	-982.24	182.32	2895.92	-2095.92	20998.37	22621.25
100	10	1000	-1227.8	227.9	3619.9	-2619.9	26247.96	28276.56

Table 24 shows the energy balance in the discharging phase. In this case, the column "Total mass" shows the necessary amount of water and ice stored in the defined conditions for thermal storage to operate the corresponding number of hours at each power level.

Table 24. Energy balance of the discharging phase as a function of net capacity

Power (MW)	Time(h)	Electrical energy (MWh)			Heat (MWh)		Total mass (t)	
Net	Discharging	Net	Pump	Turbine	HT-hx	LT-hx	Water	Ice
5	1	5	-2.73	7.73	-32.8	27.75	237.85	299.52
5	2	10	-5.46	15.46	-65.6	55.5	475.7	599.04
5	4	20	-10.92	30.92	-131.2	111	951.41	1198.08
5	6	30	-16.38	46.38	-196.8	166.5	1427.11	1797.12
5	8	40	-21.84	61.84	-262.4	222	1902.82	2396.16
5	10	50	-27.3	77.3	-328	277.5	2378.52	2995.2
100	1	100	-54.64	154.64	-656.1	555.05	4757.4	5990.65
100	2	200	-109.28	309.28	-1312.2	1110.1	9514.8	11981.3
100	4	400	-218.56	618.56	-2624.4	2220.2	19029.6	23962.61
100	6	600	-327.84	927.84	-3936.6	3330.3	28544.4	35943.91
100	8	800	-437.12	1237.12	-5248.8	4440.4	38059.2	47925.22
100	10	1000	-546.4	1546.4	-6561	5550.5	47574	59906.52

The analysis shows an imbalance between the thermal energy stored at each temperature level, not using the whole storage capacity and penalising the round-trip efficiency. Based on the balance between the thermal energy accumulated during the charging phase at various temperature levels and the thermal energy needed during the discharge phase at those same levels, each tank will have varying excess (either hot water or ice). Alternatively, one tank might be depleted, constraining the operational duration of the discharge phase. The amount of surplus thermal energy in each case (which can be used for other applications, such as heating or cooling) depends on the combination of charging and discharging operating conditions.

Table 25 shows the balance of charge-discharge operation, considering the same power in each phase ("Power in" and "Power out") and different number of charging hours ("Charging time"), in which "Time HT" and "Time LT" show the number of discharge hours available in each thermal storage tank, "Discharging Time" would be the minimum between these two values and "Excess HT and LT" shows the level of each thermal storage tank when the discharge phase concludes.

Table 25. Charging-discharging operation balance according to the number of charging hours

Power in (MW)	Power out (MW)	Charging time (h)	Time HT (h)	Time LT (h)	Discharging time (h)	Excess HT (%)	Excess LT (%)
5	5	1	0.55	0.47	0.47	17.02	0
5	5	2	1.1	0.94	0.94	17.02	0
5	5	4	2.21	1.89	1.89	16.93	0
5	5	6	3.31	2.83	2.83	16.96	0
5	5	8	4.41	3.78	3.78	16.67	0
5	5	10	5.52	4.72	4.72	16.95	0
100	100	1	0.55	0.47	0.47	17.02	0
100	100	2	1.1	0.94	0.94	17.02	0
100	100	4	2.21	1.89	1.89	16.93	0
100	100	6	3.31	2.83	2.83	16.96	0
100	100	8	4.41	3.78	3.78	16.67	0
100	100	10	5.52	4.72	4.72	16.95	0

The analysis shows a direct relationship between the energy stored during the charging phase and the energy available during the discharge phase. This relationship corresponds to the round-trip efficiency of the system, which, at this stage of the analysis, depends only on the shape of the CO_2 transcritical cycles, determined by the combinations of pressures on the high-temperature and low-temperature sides of each phase (charging and discharging), and not on the size of the plant (if components efficiency are maintained).

In all cases, the low-temperature tank (LT-tank) is completely discharged, while the high-temperature tank (HT-tank) remains at a value very close to 17% of its capacity. The round-trip efficiency, which relates the electrical energy generated during discharge to the electrical energy consumed during charging, remains constant.

5.3 Integration of geological storage

5.3.1 Preliminary analysis of the impact of the plume conditions in the surface injection and production conditions

This section presents the results of the model simulations performed. Table 26 illustrates the impact of well conditions on the CEEGS system. It shows the number of hours of discharge available in each thermal energy storage reservoir after 10 hours of charging phase, both in an open cycle and with the same net power, classified according to the simulated well conditions. For each pressure value, a different temperature range (cells in yellow) of CO_2 plume in the underground geological formation is considered, limited by the fluid characteristics, so that the supercritical state is always ensured (see Figure 8). These pressure and temperature values are directly related to the type of geological reservoir and the depth of the well. Next to each temperature value, the number of hours of hot water (orange) and ice (blue) storage is shown.

Table 26. Results of the analysis of the impact of well conditions on the CEEGS system.

1	2	Pressure [bar]													
	3	80		100		120		140		160		180		200	
		21.97	4.94	24.54	5.07	26.89	5.20	29.07	5.31	31.10	5.42	33.08	5.60	35.21	6.03
			4.51		4.63		4.75		4.85		4.95		5.12		5.51
		27.75	4.47	31.30	4.62	34.41	4.75	37.22	4.87	39.79	4.98	42.26	5.16	44.81	5.58
			4.39		4.53		4.66		4.79		4.90		5.08		5.49
		31.76	3.99	36.84	4.16	41.06	4.30	44.75	4.43	48.06	4.55	51.14	4.73	54.24	5.15
			4.22		4.40		4.56		4.70		4.83		5.02		5.47
		33.77	3.48	41.00	3.70	46.73	3.86	51.59	4.00	55.83	4.13	59.70	4.32	63.48	4.74
			3.97		4.22		4.41		4.58		4.73		4.95		5.44
		34.56	2.97	44.09	3.24	51.61	3.43	57.85	3.59	63.21	3.73	68.02	3.93	72.62	4.36
			3.64		3.98		4.23		4.43		4.62		4.87		5.40
		35.26	2.45	46.89	2.77	56.21	3.01	63.92	3.19	70.51	3.35	76.37	3.56	81.90	4.00
			3.22		3.66		3.98		4.25		4.47		4.76		5.35
		36.74	1.93	50.28	2.32	61.26	2.60	70.41	2.81	78.24	2.99	85.18	3.21	91.68	3.67
			2.69		3.26		3.68		4.02		4.29		4.63		5.29
		39.97	1.44	55.17	1.92	67.58	2.26	78.02	2.51	86.99	2.70	94.94	2.94	102.40	3.43
			2.03		2.77		3.32		3.74		4.09		4.48		5.22
		45.87	1.20	62.32	1.93	75.90	2.36	87.39	2.64	97.31	2.84	106.20	3.09	114.50	3.69
			1.21		2.20		2.90		3.43		3.85		4.31		5.14

(3) 1) CO_2 plume temperature; 2) Discharging hours available in HT-TES; 3) Discharging hours in LT-TES

The number of hours available in each thermal energy storage tank is directly related to the overall roundtrip efficiency. For comparison, considering a closed cycle, there would be 5.55 hours of available discharge in the hot water storage tank and 4.73 in the ice storage tank for each 10-hour charging phase at constant net electrical power. The system would be unbalanced since when the ice storage tank is discharged after operating the available discharge hours, there is still almost one more hour of operation in the water tank, with a level in the tank of 17.37%. It means a roundtrip efficiency range of 47.3-55.5%. An external input would be required to balance the system or to use the thermal energy in other processes to take full advantage of the stored energy.

The injection/extraction of CO_2 into the underground geological formation changes the shape of the transcritical cycles and the amount of energy stored in each reservoir. Figure 28 shows the T-s diagram of the CO_2 transcritical cycles with the system operating in closed and open cycles, with well conditions of 100 bar and 44 ºC.

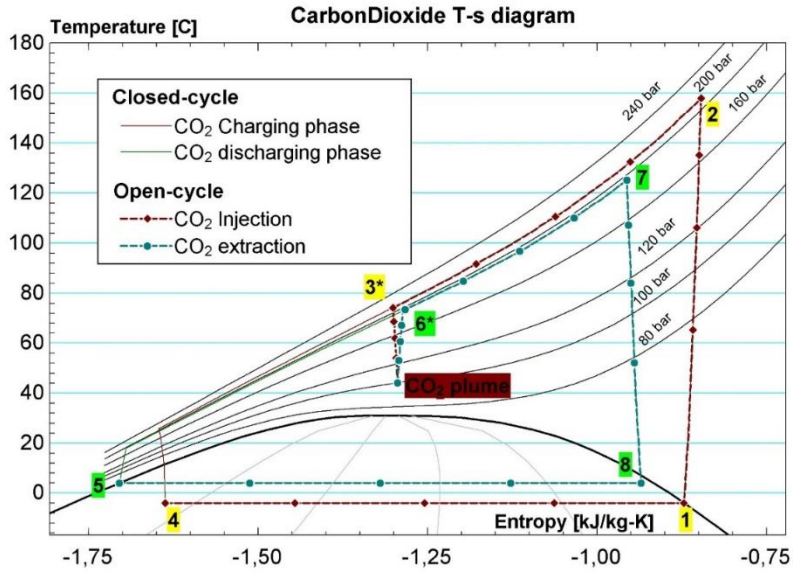

Figure 28. T-s diagram of CO_2 showing the CEEGS system operating as closed cycle and open cycle with well conditions of 100 bar and 44 °C.

One of the balanced walks of the system could be achieved with a change in the mode of operation, taking advantage of the geological storage of CO_2, since in many of the cases analysed, the number of discharge hours available in ice storage is higher than in hot water storage.

In this case, after 10 hours of charging, the system has 3.24 hours of hot water discharge available and almost 4 hours in the ice storage tank. Proper programming of the plant switching between closed and open cycle operation can balance the system, ensuring full discharge of the thermal energy stored in hot water and ice storage tanks. Balanced discharge through open-cycle operation can penalise system efficiency, depending on the well depth. Figure 29 shows the roundtrip efficiency of the system operating in an open cycle, depending on the number of hours available in the hot water tank (HT) and ice storage tank (LT).

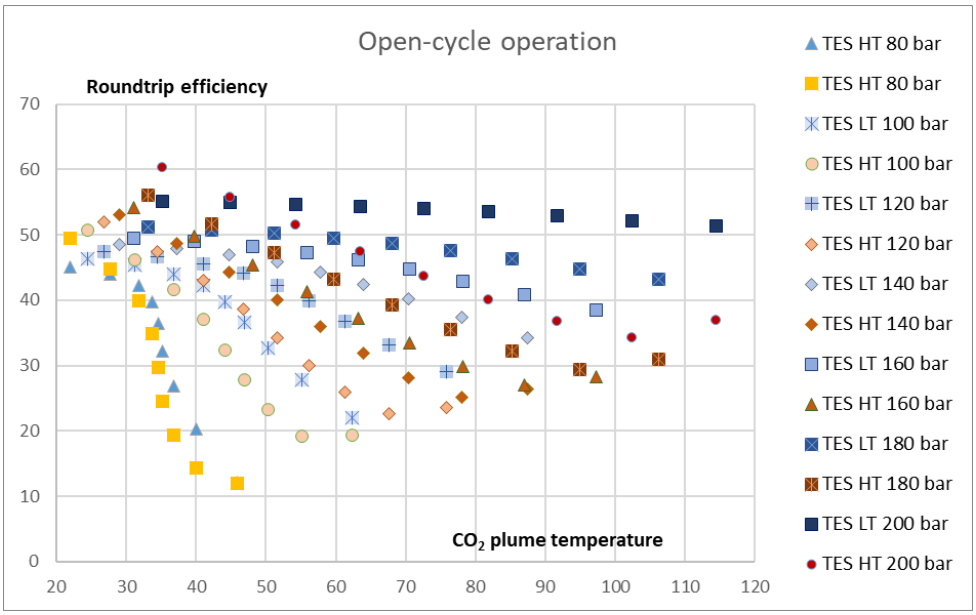

Figure 29. Roundtrip efficiency of CEEGS system operating in open cycle against CO_2 plume temperature.

Two phenomena derived from the considerations considered in the analysis can be observed in the graph. A rather flat evolution of the efficiency is observed regarding the low-temperature storage since the heat exchange conditions remain unchanged. However, a considerable drop in efficiency is observed for high-temperature storage because the heat exchanged decreases as the temperature of the underground CO_2 plume increases.

In cases of high efficiency in closed cycle operation, with pressures between 160-200 bar, the efficiency can fall from values above 50% to values in the range of 25-40%. To prevent this efficiency drop, the injection parameters are adjusted to sustain the high-temperature heat exchange conditions. Following the exchange, the CO_2 is aconditioned before injection.

5.3.2 Injection into salt cavities

This analysis follows the methodology described in section 4.3 for salt cavity injection. In addition, are assumed the following considerations:

- The charging phase's high-temperature exchange conditions (sCO_2-water) are not modified.
- At the high-temperature exchanger's (HT-hx) outlet, the CO_2 conditions are adapted before the injection.
- Injection conditions:
    - Mass flow rate 100 kg/s
    - Tube diameter 0.5 m
    - Depth of the CO_2 plume 1500 m (60 ºC, 99 bar, 283.9 kg/m^3)

The following figure shows the P-h diagram of the CO_2 transcritical cycles considering the injection in saline cavities.

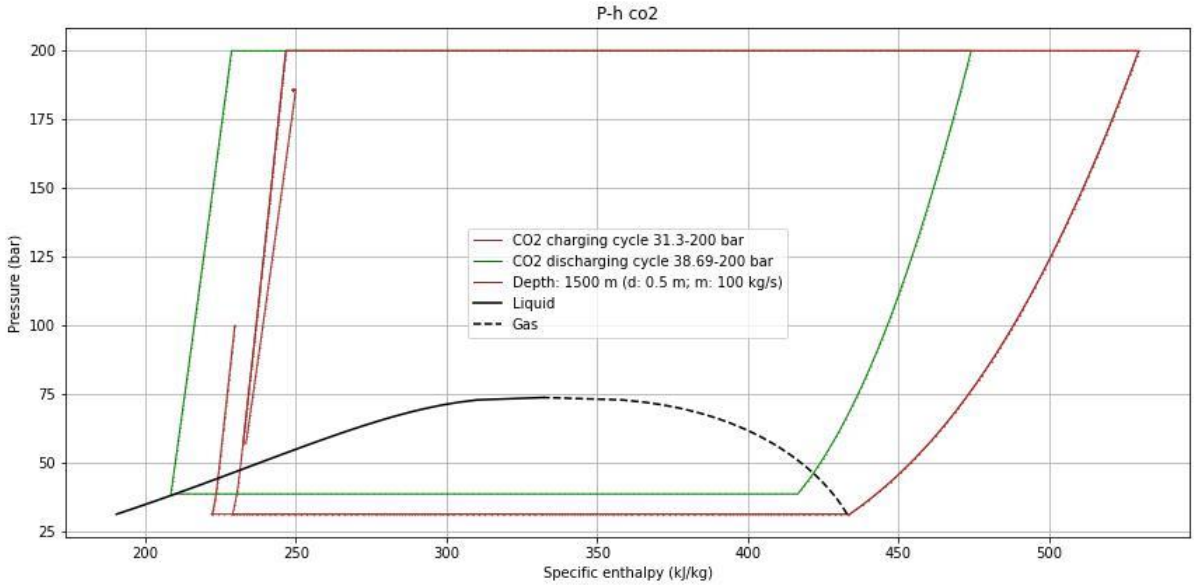

Figure 30. P-h diagram of CO_2 transcritical cycles considering the injection in saline cavities.

With the new injection considerations, the thermal energy that can be stored in the high-temperature reservoir is not penalized by the change in operating conditions, avoiding the drop in efficiency considering the high-temperature storage. In addition, the CO_2 conditions at the wellhead are low temperature, allowing it to benefit from the geothermal gain after being injected.

It is also observed that the pressure during injection increases considerably. This pressure increase could exceed the limits of the reservoir if operated at other conditions or increased depth. The following is a preliminary study of an injection with intermediate pressure controls.

5.3.3 Injection analysis considering intermediate pressure control

Different cases are considered in the injection analysis in Ebsilon Professional software, assuming a net electrical input power of 1, 5 and 100 MWe, and four injection cases: no pressure constraint, one, two and three intermediate pressure reductors/dampers.

Injection

In this analysis, the properties of the compressor and high-pressure exchanger are kept constant and equal to the results in the closed load cycle model. Only a valve has been introduced after the heat exchanger, and after it, the injection well is located.

- Injection without pressure reductors/dampers for cycle values of 1 MW. These values have been calculated for a pipe diameter of 0.09 m, resulting in fluid velocities of less than 10 m/s. CO_2 enters a liquid state, and in the section from 600 m to 900 m, it changes to a supercritical state.
- Injection without pressure reductors/dampers for cycle values of 5 MW. In this case, being a higher power cycle, the flow rate is higher than in the previous case, and since the diameter does not vary, the fluid velocity is higher. With this, the CO_2 does not pass to the supercritical state until the section from 1200 to 1500 m. These values have been calculated for a pipe diameter of 0.09 m, resulting in fluid velocities of less than 10 m/s.
- Injection without pressure reductors/dampers for cycle values of 100 MW. In this case, the increase in the pipe diameter has been considered since the velocities inside the pipe were

excessively high. These values have been calculated for a pipe diameter of 0.3 m, resulting in fluid velocities lower than 20 m/s.

Table 27. Injection (diameter 0.09-0.3 m)

Power in (MWe)	Depth (m)	Pressure (bar)	Temperature (ºC)	Enthalpy (kJ/kg)	Quality (%)	State
Valve	Inlet	240	29.8	252.26	0	Liquid
	Outlet	90	22.7	252.2	0	Liquid
1	Surface	90	22.7	252.2	0	Liquid
	300	113.92	24	250.73	0	Liquid
	600	138.30	27.3	255.40	0	Liquid
	900	162.72	32.0	263.25	100	Supercritical
	1200	186.98	37.8	273.53	100	Supercritical
	1500	210.92	44.4	285.62	100	Supercritical
	1800	234.46	51.7	298.99	100	Supercritical
5	Surface	90	22.7	252.25	0	Liquid
	300	101.93	23.7	252.35	0	Liquid
	600	114.25	25.0	253.45	0	Liquid
	900	126.81	26.7	255.51	0	Liquid
	1200	139.51	28.7	258.48	0	Liquid
	1500	152.24	31.0	262.33	100	Supercritical
	1800	164.92	33.7	267.01	100	Supercritical
100	Surface	90	22.7	252.25	0	Liquid
	300	104.67	23.9	252.25	0	Liquid
	600	119.83	25.0	252.37	0	Liquid
	900	135.44	26.1	252.59	0	Liquid
	1200	151.4	27.1	252.92	0	Liquid
	1500	167.87	28.0	253.36	0	Liquid
	1800	184.62	28.9	253.90	0	Liquid

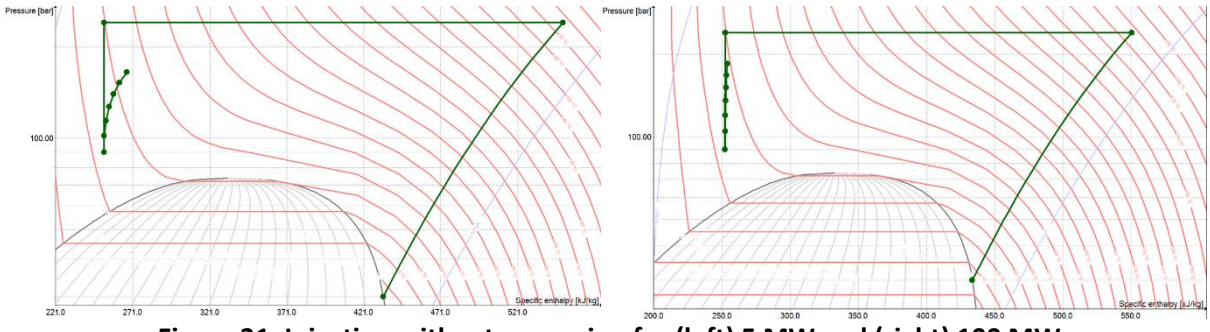

Figure 31. Injection without expansion for (left) 5 MW and (right) 100 MW

Injection with one intermediate pressure control

In this case, one pressure reduction/damper is located halfway down the injection depth to mitigate possible problems related to the phase change inside the injection tube. The pressure set at the outlet of the expander is the minimum possible pressure to remain in the liquid state before entering the two-phase zone.

- Injection with one pressure damper for cycle values of 1 MW. In this case, before entering the pressure damper, it is already in the supercritical state, and after it, it passes to the liquid state, although it changes phase again in the section from 1200 to 1500m. These values have been calculated for a pipe diameter of 0.09 m, resulting in fluid velocities of less than 10 m/s.
- Injection with one pressure damper for cycle values of 5 MW. Thanks to the pressure profile control, the injected fluid does not change state, and the pressure at the bottom is similar to the pressure at the beginning of the pipe. These values have been calculated for a pipe diameter of 0.09 m, resulting in fluid velocities of less than 10 m/s.
- Injection with one pressure damper for cycle values of 100 MW. For this power, the liquid state is always maintained, and the pressures at the bottom are similar to those at the pipe inlet. These values have been calculated for a pipe diameter of 0.3 m, resulting in fluid velocities of less than 20 m/s.

Table 28. Injection with one intermediate pressure control (diameter: 0.09-0.3 m)

Power in (MWe)	Depth (m)	Pressure (bar)	Temperature (°C)	Enthalpy (kJ/kg)	Quality (%)	State
Valve	Inlet	240	29.8	252.26	0	Liquid
	Outlet	90	22.6	252.25	0	Liquid
1	Surface	90	22.6	252.25	0	Liquid
	300	113.9	24	250.73	0	Liquid
	600	138.30	27.3	255.40	0	Liquid
	900	162.72	32.0	263.25	100	Supercritical
	Damper outlet	61	22.2	263.24	0	Liquid
	1200	82.05	29.4	279.33	0	Liquid
	1500	102.29	37.0	296.42	100	Supercritical
	1800	121.45	45.2	314.22	100	Supercritical
5	Surface	90	22.6	252.25	0	Liquid
	300	101.93	23.7	252.35	0	Liquid
	600	114.25	25.5	253.45	0	Liquid
	900	126.81	26.7	255.51	0	Liquid
	Damper outlet	58	20.0	255.50	0	Liquid
	1200	67.83	22.3	259.31	0	Liquid
	1500	77.57	24.9	263.95	0	Liquid
	1800	87.11	27.7	269.41	0	Liquid
100	Surface	90	22.6	252.25	0	Liquid
	300	104.67	23.9	252.25	0	Liquid
	600	119.83	25.0	252.37	0	Liquid
	900	135.44	26.0	252.59	0	Liquid
	Damper outlet	56	19.0	252.58	0	Liquid
	1200	69.19	20.8	253.00	0	Liquid
	1500	82.94	22.4	253.52	0	Liquid
	1800	97.18	23.9	254.13	0	Liquid

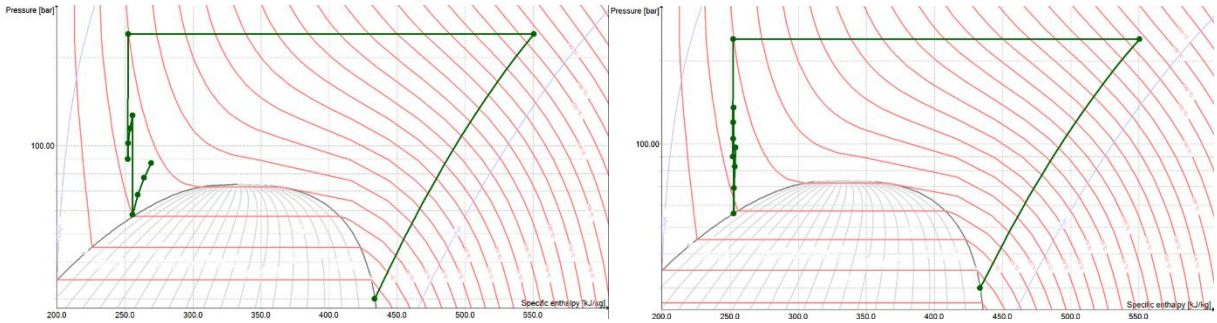

Figure 32. Injection with one expander for: left) 5 MW right) 100 MW

Injection with two pressure control elements

Another pressure damper is added to further study the different behaviours of the fluid in the injection well. The dampers are distributed equidistantly placed along the pipe (1/3 apart from each other).

- Injection with two pressure dampers for 1 MW cycle values. By adding two pressure dampers, it avoids the early phase change that occurred previously between 600 and 900m, although phase changes persist, this time between 900 and 1200m and between 1200 and 1500m after leaving the second expander. These values have been calculated for a pipe diameter of 0.09 m, resulting in fluid velocities of less than 10 m/s.
- Injection with two pressure dampers for cycle values of 5 MW. Although the CO_2 state can be maintained with only one pressure damper, adding an additional pressure control element generates a more homogenous pressure profile with an outlet pressure similar to (and lower) than the inlet. These values have been calculated for a pipe diameter of 0.09 m, resulting in fluid velocities of less than 10 m/s.
- Injection with two pressure dampers for cycle values of 100 MW. This variation has a similar behaviour to the case with one expander, only that, in general, the pressures are lower along the pipe. These values have been calculated for a pipe diameter of 0.3 m, resulting in fluid velocities lower than 20 m/s.

Table 29. Injection with two pressure controls (diameter: 0.09-0.3 m)

Power in (MWe)	Depth (m)	Pressure (bar)	Temperature (ºC)	Enthalpy (kJ/kg)	Quality (%)	State
Valve	Inlet	240	29.8	252.26	0	Liquid
	Outlet	90	22.6	252.2	0	Liquid
1	Surface	90	22.6	252.2	0	Liquid
	300	113.92	24	250.79	0	Liquid
	600	138.30	27.3	255.47	0	Liquid
	Damper outlet	61	20.4	255.38	0	Liquid
	900	83.14	26.5	267.22	0	Liquid
	1200	104.88	33.3	280.62	100	Supercritical
	Damper outlet	67	26.4	280.67	0	Liquid
	1500	86.07	34.1	299.5	100	Supercritical
	1800	103.97	42.2	319.36	100	Supercritical
5	Surface	90	22.6	252.25	0	Liquid
	300	101.93	23.7	252.35	0	Liquid
	600	114.25	25.0	253.45	0	Liquid
	Damper outlet	60	19.7	253.44	0	Liquid

	900	70.32	21.8	256.15	0	Liquid
	1200	80.73	24.1	259.73	0	Liquid
	Damper outlet	67	22.3	259.73	0	Liquid
	1500	76.63	24.9	264.37	0	Liquid
	1800	86.05	27.6	269.83	0	Liquid
100	Surface	90	22.6	252.2	0	Liquid
	300	104.67	23.9	252.25	0	Liquid
	600	119.83	25.0	252.37	0	Liquid
	Damper outlet	56	18.9	252.36	0	Liquid
	900	69.23	20.7	252.66	0	Liquid
	1200	83.03	22.3	253.06	0	Liquid
	Damper outlet	56.5	19.2	253.05	0	Liquid
	1500	69.64	21.0	253.59	0	Liquid
	1800	83.32	22.7	254.22	0	Liquid

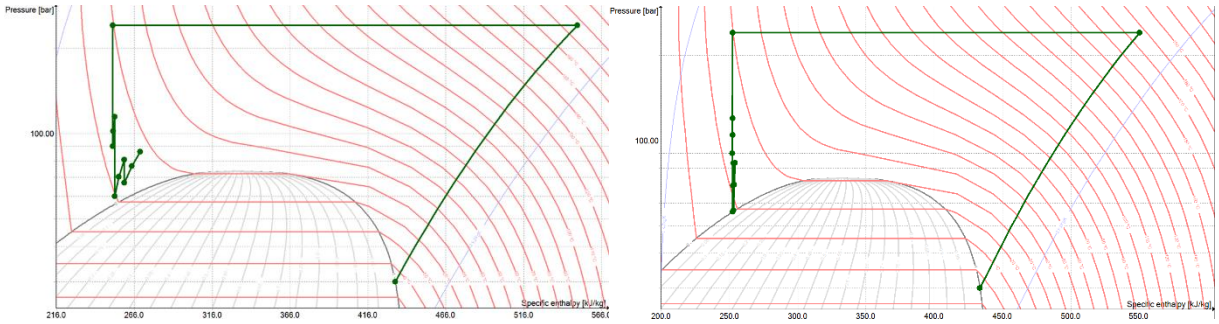

Figure 33. Injection with two pressure controls for: left) 5 MW right) 100 MW

6. Heat exchanger's preliminary design

The preliminary design of low-temperature latent heat exchangers (LT-hx) and high-temperature sensible heat exchangers (HT-hx) is considered for 5 and 100 MWe plant sizes, which can operate in both charging and discharging phases. Preliminary sizing of the exchangers is performed considering the operating conditions of the discharge cycle.

In the high-temperature exchanger, the sensible heat exchange of CO_2 under supercritical conditions and water is considered under the abovementioned conditions. In the case of the low-temperature exchanger, a first approximation is made, maintaining the conditions previously analyzed, CO_2 phase change in subcritical conditions at a temperature close to 0 ºC. For this purpose, R-22 is considered as the other fluid involved. The assumptions made in the preliminary design of the heat exchangers are shown below.

Table 30. Operating conditions of LT-hx (R-22/CO_2) and HT-hx (water/sCO_2) heat exchangers

		5 MWe		100 MWe	
HT-hx		Tube Side	Shell Side	Tube Side	Shell Side
Tin/Tout	(ºC)	29.04/159	161/30	29.04/159	161/30
Pin/Pout	(ºC)	240/240	12/12	240/240	12/12
Mass flow	(kg/h)	382680	181299	7696800	3643812
Duty	MWth	29.1		585.1	
LT-hx		Tube Side	Shell Side	Tube Side	Shell Side
Tin/Tout	(ºC)	15.65/6.556	-1.86/10.65	15.65/6.556	-1.86/10.65
Pin/Pout	(ºC)	40/40	4.029/4.029	40/40	4.029/4.029
Mass flow	(kg/h)	382680	398880	7696800	8023680
(kg/h)	MWth	24.11		484.8	

In the design of the exchangers for 5 MW and 100 MW cycles, the D-type distribution head is selected, as it is suitable for high-pressure applications, and the W-type closing head, due to the thermal and mechanical stresses. Table 31 provides the main assumptions taken into account in the simulation.

Table 32. Assumptions for heat exchangers simulation in Aspen

	High Temperature-hx		**Low temperature-hx**	
	Tube Side	Shell Side	Tube Side	Shell Side
Fouling factor (m^2K/kW)	0.2	0.1	0.2	0.2
Permissible pressure drop (bar)	0.5	0.9	0.5	0.5
Tube Layout	30º		30º	
Thermodynamic properties package	PENG-ROBINSON	REFPROF	SRK	REFPROF

Their heat exchange has been calculated and optimised, distributing the thermal power exchanged and avoiding the crossovers. In the appendix, technical characteristics and drawings with the distribution of the heat exchangers and the layout of the tubes are presented in detail. Figure 34 and Figure 35 show the temperature distribution through the heat exchangers' sets for both sizes.

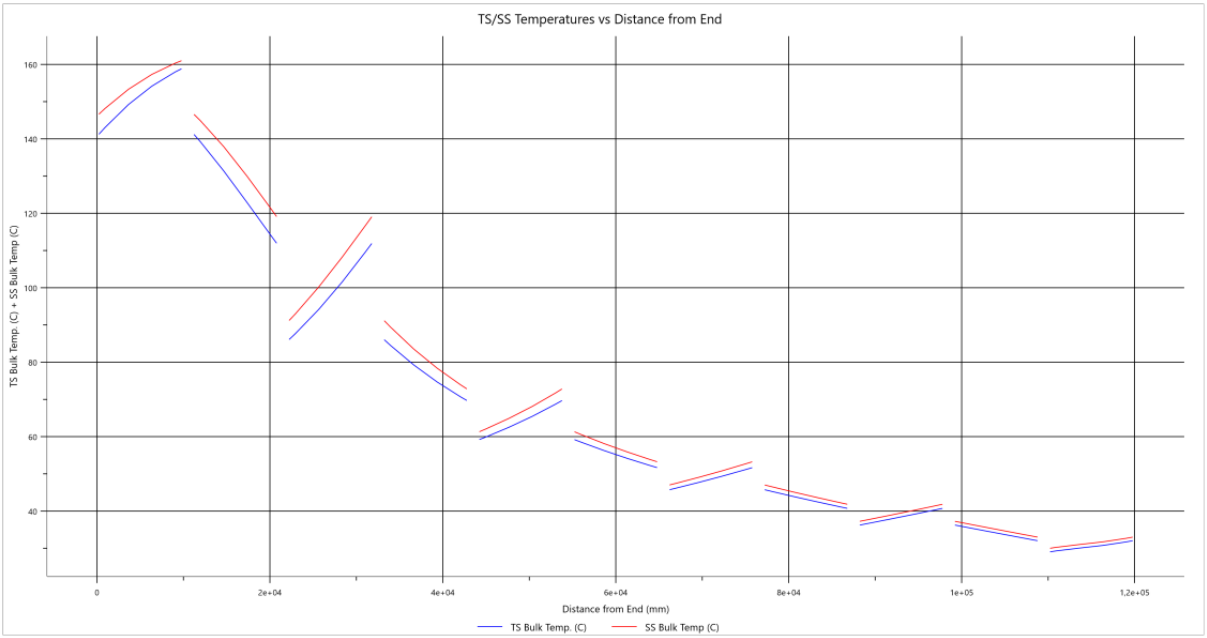

Figure 36. T-distance diagram for HT-hx in 5 MWe power level

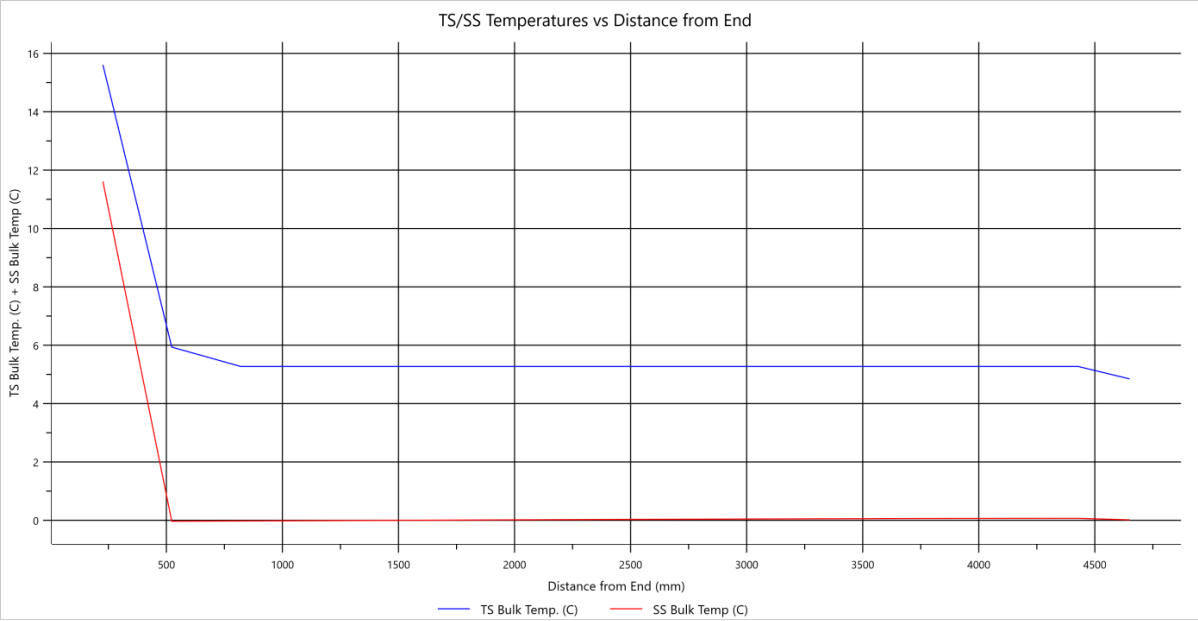

Figure 37. T-distance diagram for LT-hx in 100 MWe power level

The exchangers corresponding to the 5 MWe cycle consist of a single unit, while those of the 100 MWe power cycle are divided into four units in each case. Each has a different configuration regarding the number of parallel and series casings that optimises the exchange. The main global results are shown in Table 33.

Table 34. Main results in preliminary heat exchangers design

	Units	HT-hx	sCO_2-Water	LT-hx	sCO_2-R22
Power level	MWe	5	100	5	100
Units	Number	1	4	1	4
Duty	MW/Unit	28	150	24.9	130
Total duty	MW	28	600	24.9	520
Configuration	(Paralell x Series)	3x11	12x10	4x2	10x2
Shells	Number	33	120	8	20
Shell cost	M USD/shell	0.25	0.52	0.25	0.73
Total price	M USD	8.2	62.4	1.98	14.7
Weight-shells	ton	5.82	12.66	4.44	10.94
Total weight	ton	28.24	72.53	27.35	96.9
Effective surface	m^2/shell	1516.7	2865.2	946.3	2312.6
	m^2/unit	50050	43823	7570.8	46252.6
Total effective surface	m^2	50050	343823	7570	184960

The result is the successful preliminary design of two heat exchangers, at two different power levels each, that allow effective exchange in the temperature and pressure range of CO_2 transcritical cycles. As can be seen in the preliminary design reports of the heat exchangers located in the Annex, which include the technical characteristics and plans, the simulations have taken into account the maximum pressures of shells and tubes and the value of the Overall transfer coefficient in each case falls within the range of 150-800 W/m^2K, considered in similar exchangers [25,26].

7. Main Conclusions

The first period of task 3.1 has evolved satisfactorily, and relevant results regarding the layouts' definitions and parameters have been obtained. They will allow advancing in the next steps within task 3.1 and the related tasks in WP3 and WP4. No delays or deviations are identified regarding the planned activities.

The main conclusions derived from the execution of task 3.1 in this first period are the following:

a) Related to the definition of the reference layouts integration

- The analysis of the characteristics of thermal exchanges and the impact of CO_2 pressure values on the high-pressure side, along with the effects of various integrations and operational strategies on components, shows that effective integrations can be obtained, with round-trip efficiency results reaching 57%.

- These high-efficiency values are achieved through thermal storage at temperatures above 150°C on the high-temperature side and latent heat thermal storage at 0°C, which can be integrated with industrial systems. Effective integration with the temperature profiles of heat exchangers is crucial for plant efficiency. In the context of CO_2 transcritical cycles, using ice for low-temperature thermal storage and hot water for high-temperature storage proves highly effective. This is due to the excellent thermal properties and environmental characteristics of these materials and their compatibility with the operating range of the CO_2 transcritical cycle. Latent heat is utilized to store thermal energy at low temperatures through the phase change of ice, aligning with CO_2 evaporation during charging and CO_2 condensation during discharge. On the high-temperature side, liquid water alters its temperature, storing thermal energy as sensible heat within a range defined by the cooling and heating curves of supercritical CO_2 during the charging and discharging phases.

- The high values of round-trip efficiency correspond to higher CO_2 pressure values during both the charging and discharging phases, imposing the thermodynamic cycle's shape. This relationship remains consistent regardless of the plant's size. The high-efficiency cases, above 50%, include all combinations of pressure on the high-temperature side of the charging and discharging phase above 160 bar, and some combinations for even higher pressures, such as the case of 140 bar in discharging for 180-240 bar in the charging phase and the case of 120 bar in discharging for 220-240 bar in the charging phase.

- As the charging phase progresses, the high-temperature thermal energy storage (HT-TES) and low-temperature thermal energy storage (LT-TES) tanks may not accumulate thermal energy in proportion to the discharge requirements of the CO_2 transcritical cycle. In practical terms, the hot water tank might store thermal energy suitable for different operating hours compared to the ice tank. Consequently, one of the tanks will discharge before reaching a "maximum" or "minimum" round-trip efficiency. High efficiency is achieved with a balanced design and operational strategies. External heat sources can be implemented to harmonize the discharge phase of the two storage tanks. The surplus thermal energy available, suitable for various applications like heating or cooling, is contingent upon the specific combination of charging and discharging operational parameters in each scenario.

b) Integration with underground geological formations

- Integrating the injection after completing the high-temperature exchange (sCO_2-water) during the charging phase and adjusting the conditions based on the depth of the geological formation, the thermal energy stored in each reservoir is similar to that of the closed-cycle operation. This approach avoids roundtrip efficiency penalties (drops of up to 20%) and enables employing the geothermal gain in the underground geological formation, as CO_2 is injected at low-temperature conditions.

- The preliminary approach in this deliverable uses a methodology for saline cavities yields to define the global cycle reference conditions. It results in a steady increase in pressure during injection. This pressure increase could exceed the limits of the reservoir if operated at other conditions during variable operation or if the design depth was increased. A study on injection is conducted by implementing intermediate pressure controls, demonstrating that CO_2 conditions could be managed during the injection process. It shows how an efficient control of the pressure can be obtained, adequate to the operation characteristics of operation of the global concept.

c) Preliminary design of heat exchangers

- To identify the adequateness and feasibility of the defined framework regarding the heat transfer processes, the preliminary design of low-temperature latent heat exchangers (LT-hx) and high-temperature sensible heat exchangers (HT-hx) for a 5 and 100 MWe power plant, which can operate in both charging and discharging phases, has been performed.

- In the high-temperature exchanger, the sensible heat exchange of CO_2 under supercritical conditions and water is considered under the abovementioned conditions. In the case of the low-temperature exchanger, a first approximation is made, maintaining the conditions previously analyzed of CO_2 phase change under subcritical conditions at a temperature close to 0 ºC.

- In the simulations developed, the maximum shell and tube pressures have been taken into account, and the value of the global transfer coefficient in each case falls within the adequate range of 150-800 W/m^2K.

- The results of the preliminary design of two heat exchangers are satisfactory at the two different power ratings. They allow an adequate exchange in the temperature and pressure range of the CO_2 transcritical cycles. The technical characteristics and drawings of each heat exchanger are shown in the annexe.

The following activities within task 3.1 comprise the analysis of the components' integration and design and their effect on the design and parameters of the cycle in an iterative process. They will be presented in month 24 within D3.5.

Nomenclature

Abbreviations

CAES	Compressed Air Energy Storage
CCS	Carbon Capture and Storage
CEEGS	CO_2-based Electrothermal Energy and Geological Storage
CO_2	Carbon Dioxide
CSP	Concentrated Solar Power
EES	Engineering Equation Solver

EOR	Enhanced oil recovery
ETES	Electrothermal Energy Storage
HE	Heat Engine
HP	Heat Pump
hx	Heat exchanger
HT	High temperature
HTF	Heat Transfer Fluid
LT	Low temperature
PHS	Pumped Hydropower Storage
PV	Photovoltaic
TEES	Thermoelectrical Energy Storage
TEMA	Tubular Exchanger Manufacturers Association
TES	Thermal Energy Storage
TRL	Technological Readiness Level

Units

P	Pressure, bar
$\dot{Q}$	Heat, kW
T	Temperature, ºC
$\dot{W}$	Power, kW
h	Specific enthalpy, kJ/kg
s	Specific entropy, kJ/kg-K
t	Time, hours

Greek symbols

η	efficiency

Subscripts and superscripts

ele	electric
hx	Heat Exchanger
th	thermal

References

[1] Mercangöz M, Hemrle J, Kaufmann L, Z'Graggen A, Ohler C. Electrothermal energy storage with transcritical CO2 cycles. Energy 2012;45:407–15. https://doi.org/10.1016/j.energy.2012.03.013.

[2] Svensson R, Odenberger M, Johnsson F, Strömberg L. Transportation systems for CO2 - Application to carbon capture and storage. Energy Convers Manag 2004;45:2343–53. https://doi.org/10.1016/j.enconman.2003.11.022.

[3] Carro A, Chacartegui R, Ortiz C, Carneiro J, Becerra JA. Integration of Energy Storage Systems based on transcritical CO2: Concept of CO2 based Electrothermal Energy and Geological Storage. Energy 2021:121665. https://doi.org/10.1016/J.ENERGY.2021.121665.

[4] Carro A, Chacartegui R, Ortiz C, Carneiro J, Becerra JA. Energy Storage System based on transcritical CO2 cycles and geological storage. Appl Therm Eng 2021;193:116813. https://doi.org/10.1016/j.applthermaleng.2021.116813.

[5] Fernandez R, Chacartegui R, Becerra A, Calderon B, Carvalho M. Transcritical carbon dioxide charge-discharge energy storage with integration of solar energy. Journal of Sustainable Development of Energy, Water and Environment Systems 2019;7:444–65. https://doi.org/10.13044/j.sdewes.d6.0235.

[6] Morandin M, Maréchal F, Mercangöz M, Buchter F. Conceptual design of a thermo-electrical energy storage system based on heat integration of thermodynamic cycles - Part A: Methodology and base case. Energy 2012;45:375–85. https://doi.org/10.1016/j.energy.2012.03.031.

[7] Yan J, Zhang X. Application and development of dynamic ice slurry technology. 2010 International Conference on Mechanic Automation and Control Engineering 2010:1441–4. https://doi.org/10.1109/MACE.2010.5536141.

[8] Global Status of CCS Report: 2020 - Global CCS Institute n.d. https://www.globalccsinstitute.com/resources/publications-reports-research/global-status-of-ccs-report-2020/ (accessed March 29, 2023).

[9] EES: Engineering Equation Solver | F-Chart Software : Engineering Software n.d. http://fchartsoftware.com/ees/ (accessed November 23, 2020).

[10] Span R, Wagner W. A new equation of state for carbon dioxide covering the fluid region from the triple-point temperature to 1100 K at pressures up to 800 MPa. J Phys Chem Ref Data 1996;25:1509–96. https://doi.org/10.1063/1.555991.

[11] Vesovic V, Wakeham WA, Olchowy GA, Sengers J V., Watson JTR, Millat J. The Transport Properties of Carbon Dioxide. J Phys Chem Ref Data 1990;19:763–808. https://doi.org/10.1063/1.555875.

[12] Chase MW, Jr. NIST-JANAF Themochemical Tables, Fourth Edition. J Phys Chem Ref Data, Monograph 9 1998:1–1951.

[13] Kestin J, Sengers J V., Kamgar parsi B, Sengers JMHL. Thermophysical Properties of Fluid H2O. J Phys Chem Ref Data 1984;13:175–83. https://doi.org/10.1063/1.555707.

[14] Coles WD. Experimental Determination of Thermal Conductivity of Low-Density Ice. 1954.

[15] Wagner W, Pruß A. The IAPWS formulation 1995 for the thermodynamic properties of ordinary water substance for general and scientific use. J Phys Chem Ref Data 2002;31:387–535. https://doi.org/10.1063/1.1461829.

[16] Bell IH, Wronski J, Quoilin S, Lemort V. Pure and pseudo-pure fluid thermophysical property evaluation and the open-source thermophysical property library coolprop. Ind Eng Chem Res 2014;53:2498–508. https://doi.org/10.1021/IE4033999/SUPPL_FILE/IE4033999_SI_002.ZIP.

[17] STEAG EBSILON n.d. https://www.ebsilon.com/de/ (accessed October 16, 2023).

[18] Wagner W, Cooper JR, Dittmann A, Kijima J, Kretzschmar HJ, Kruse A, et al. The IAPWS industrial formulation 1997 for the thermodynamic properties of water and steam. J Eng Gas Turbine Power 2000;122:150–80. https://doi.org/10.1115/1.483186.

[19] Huber ML, Lemmon EW, Bell IH, McLinden MO. The NIST REFPROP Database for Highly Accurate Properties of Industrially Important Fluids. Ind Eng Chem Res 2022;61:15449–72. https://doi.org/10.1021/ACS.IECR.2C01427.

[20] Aspen Plus | Leading Process Simulation Software | AspenTech n.d. https://www.aspentech.com/en/products/engineering/aspen-plus (accessed October 30, 2023).

[21] Aspen HYSYS | Process Simulation Software | AspenTech n.d. https://www.aspentech.com/en/products/engineering/aspen-hysys (accessed October 30, 2023).

[22] Aspen Properties | Improve Accuracy | AspenTech n.d. https://www.aspentech.com/en/products/engineering/aspen-properties (accessed October 27, 2023).

[23] Aspen Exchanger Design and Rating (EDR) | AspenTech n.d. https://www.aspentech.com/en/products/engineering/aspen-exchanger-design-and-rating (accessed October 30, 2023).

[24] TEMA | Tubular Exchanger Manufacturers Association n.d. https://tema.org/ (accessed October 30, 2023).

[25] Krishna AB, Jin K, Ayyaswamy PS, Catton I, Fisher TS. Modeling of Supercritical CO2 Shell-and-Tube Heat Exchangers Under Extreme Conditions. Part I: Correlation Development. J Heat Transfer 2022;144. https://doi.org/10.1115/1.4053510/1131190.

[26] Krishna AB, Jin K, Ayyaswamy PS, Catton I, Fisher TS. Modeling of Supercritical CO2 Shell-and-Tube Heat Exchangers Under Extreme Conditions: Part II: Heat Exchanger Model. J Heat Transfer 2022;144. https://doi.org/10.1115/1.4053511/1131192.